CHALMERS
UNIVERSITY OF TECHNOLOGY

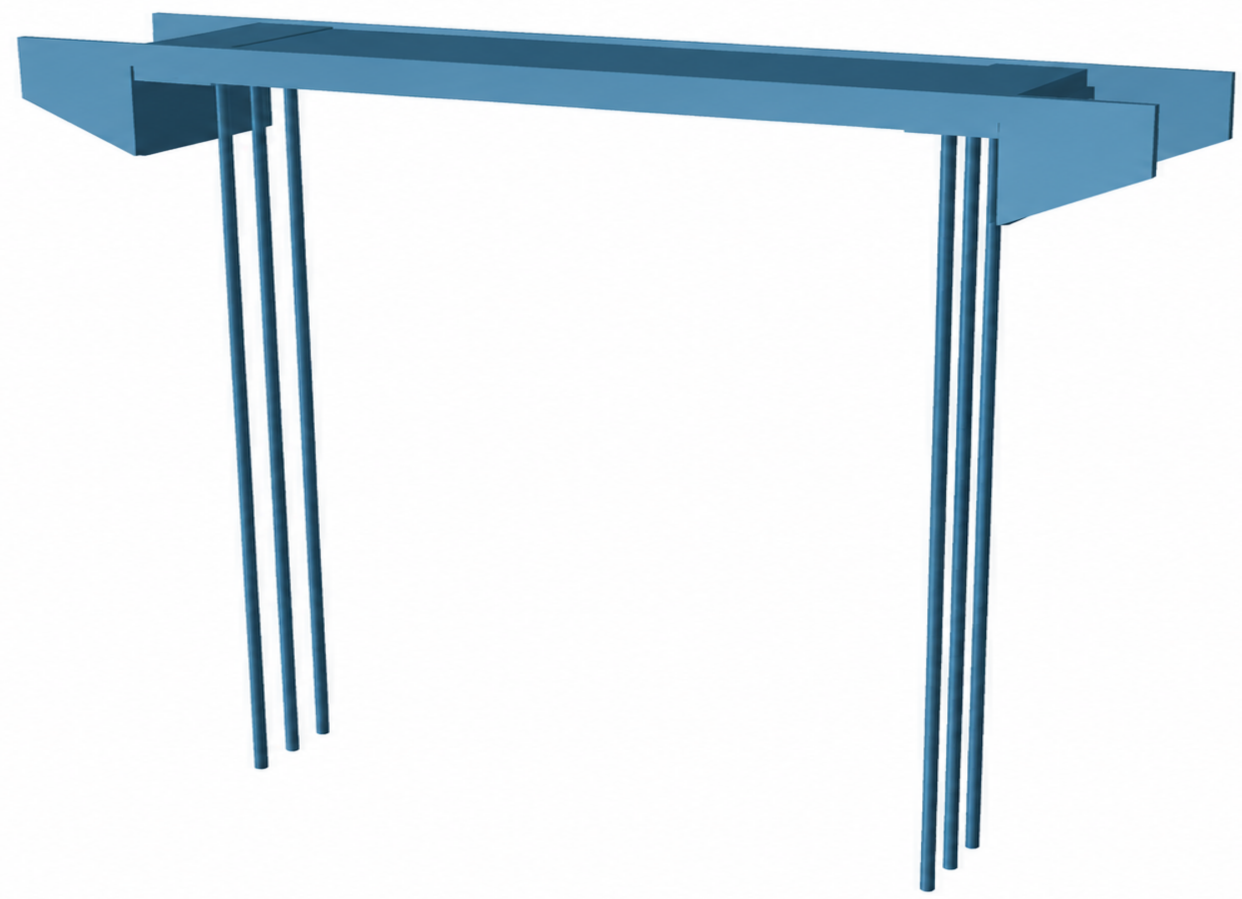

Impact of pile head restraint and soil stiffness on the response of steel piles for integral abutment bridges

Master's thesis in Master Programme Structural Engineering and Building Technology

SOFIE ALMAR
LYDIA BINBACH

DEPARTMENT OF ARCHITECTURE AND CIVIL ENGINEERING
CHALMERS UNIVERSITY OF TECHNOLOGY
Gothenburg, Sweden 2026
www.chalmers.se

Master's thesis 2026

Impact of pile head restraint and soil stiffness on the response of steel piles for integral abutment bridges

SOFIE ALMAR

LYDIA BINBACH

Department of Architecture and Civil Engineering
Civil Engineering
Chalmers University of Technology
Gothenburg, Sweden 2026

Impact of pile head restraint and soil stiffness on the response of steel piles for integral abutment bridges

SOFIE ALMAR
LYDIA BINBACH

Supervisors: Max Fredriksson and Samuel Wiik, Inhouse Tech
Joosef Leppänen, Chalmers Division of Structural Engineering
Examiner: Jelke Dijkstra, Division of Geology and Geotechnics

Master's Thesis 2026
Department of Architecture and Civil Engineering
Division of Geology and Geotechnics
Chalmers University of Technology
SE-412 96 Gothenburg
Telephone +46 31 772 1000

Cover: Integrated abutment bridge modelled in BRIGADE/Plus

Typeset in LaTeX
Printed by Chalmers Reproservice
Gothenburg, Sweden 2026

Impact of pile head restraint and soil stiffness on the response of steel piles for integral abutment bridges

SOFIE ALMAR
LYDIA BINBACH
Department of Architecture and Civil Engineering
Chalmers University of Technology

Abstract

Integral abutment bridges are commonly designed using simplified pile models where the pile is treated as an isolated structural element with a free pile head. To better represent the actual structural behaviour, global buckling analysis can be used as an alternative modelling approach, where stabilisation from the surrounding soil and the integrated bridge system is considered. The purpose of this study is therefore to evaluate whether alternative modelling approaches can provide a more realistic estimation of axial pile capacity in integral abutment bridges.

The study combines literature review, case study and finite element modelling. A finite element model was developed in BRIGADE/Plus and verified against hand calculations using simplified single pile models. The analyses were gradually extended to include soil resistance, transverse loading, and different boundary conditions. Both single piles and piles integrated into the bridge system were analysed under two different soil conditions to evaluate force distribution, bending moments, buckling behaviour, and pile capacity.

The results show significant differences in structural behaviour depending on soil conditions and model assumptions. The piles embedded in friction soil developed a higher axial capacity than the piles surrounded by soft clay. Compared with the isolated pile models, the piles integrated into the bridge system generally exhibited an increased capacity due to redistribution of internal forces and the sequential formation of plastic hinges. The results also indicate that simplified assumptions with free pile heads may underestimate the stabilising effect provided by the surrounding structural system.

The study demonstrates that modelling assumptions regarding soil stiffness and pile restraint significantly influence the predicted pile capacity in integral abutment bridges. Simplified single pile models may therefore underestimate the structural capacity of piles interacting with the bridge system. The results indicate that soil-structure interaction and restrained pile behaviour should be considered in non-linear analyses of integral abutment bridges, particularly when evaluating ultimate limit states and buckling behaviour.

Keywords: Integral abutment bridge, structural behaviour

Acknowledgements

We would like to thank our supervisors Max Fredriksson and Samuel Wiik at Inhouse Tech for their valuable feedback, expertise, and continuous guidance throughout this master's thesis. We are sincerely grateful to Inhouse Tech for welcoming us into the company and providing an inspiring workspace during our project.

We would also like to express our appreciation to Jelke Dijkstra and Joosef Leppänen at Chalmers University of Technology for their supervision and academic support.

Finally, we wish to thank our families and friends for their encouragement and support throughout these five challenging and rewarding years of study toward becoming civil engineers.

Sofie Almar & Lydia Binbach
Gothenburg, June 2026

List of acronyms

Below is the list of acronyms that have been used throughout this thesis listed in alphabetical order:

FE	Finite Element
HC	Hand Calculations
LM1	Load Model 1
N/A	Not Available
NLGEOM	Geometric Nonlinearity
SLS	Serviceability Limit State
ULS	Ultimate Limit State

Nomenclature

Below is the nomenclature of parameters and variables that have been used throughout this thesis.

Parameters

A	Cross-sectional area of steel pile
D	Outer diameter of steel pile
D_i	Inner diameter of steel pile
E_s	Young's modulus of steel
I	Moment of inertia
L	Pile length
L_{cr}	Critical buckling length
W_{el}	Elastic section modulus
W_{pl}	Plastic section modulus
f_{yd}	Design yield strength of steel
$k_d d$	Subgrade modulus
l_k	Critical buckling length
t	Wall thickness of tubular pile
γ	Unit weight
γ_m	Model factor
ϕ	Friction angle
δ_f	Fictitious initial imperfection
δ_h	Geometric initial imperfection
δ	Total initial imperfection

Variables

M	Bending moment
ΔM	Additional bending moment of horizontal force
N	Normal force
N_{max}	Normal force capacity
$N_{y,soil}$	Normal force where soil yields
$N_{y,steel}$	Normal force where steel yields
V	Transverse force
Q_d	Limit pressure $[kN/m]$
q_d	Limit pressure $[kN/^2]$

Contents

List of Figures

List of Tables

1
Introduction

Integral abutment bridges have become increasingly common in modern bridge engineering due to their jointless design, reduced maintenance needs, and favourable structural performance. Despite these advantages, the interaction between piles, the surrounding soil, and the superstructure introduces complex behaviour that may not be fully represented in conventional pile design approaches. This thesis investigates the structural behaviour of steel piles in integral abutment bridges from a system-level perspective, with the aim of developing a more realistic and material-efficient design approach.

1.1 Background

Integral abutment bridges are a common bridge type built to facilitate Sweden's infrastructure. The structure is a jointless bridge design in which the abutments consist of steel tubular piles that are cast directly into the superstructure and driven to the bedrock. Given these fixity conditions, the piles act integrally with the bridge structure. The bridge is further stabilised by end screens and wing walls, which are surrounded by filler material.

The calculations for steel pile design are typically performed by treating the pile as an isolated component, without stabilisation from the surrounding system, and with a free pile head. This method neglects the soil-structure interaction of the bridge system, and the fact that the pile is cast into the bridge deck. As a result, the design is assumed to be conservative, where the capacity of the pile is underestimated and the safety margin becomes higher than necessary. This may lead to oversized pile dimensions and inefficient use of materials.

To investigate pile design in terms of realistic structural and geotechnical behaviour, global buckling analysis can be considered as an alternative method. This approach accounts for the stabilisation of the entire bridge system and the interaction with the surrounding soil.

A simplified sketch of the bridge can be seen in Figures 1.1 and 1.2.

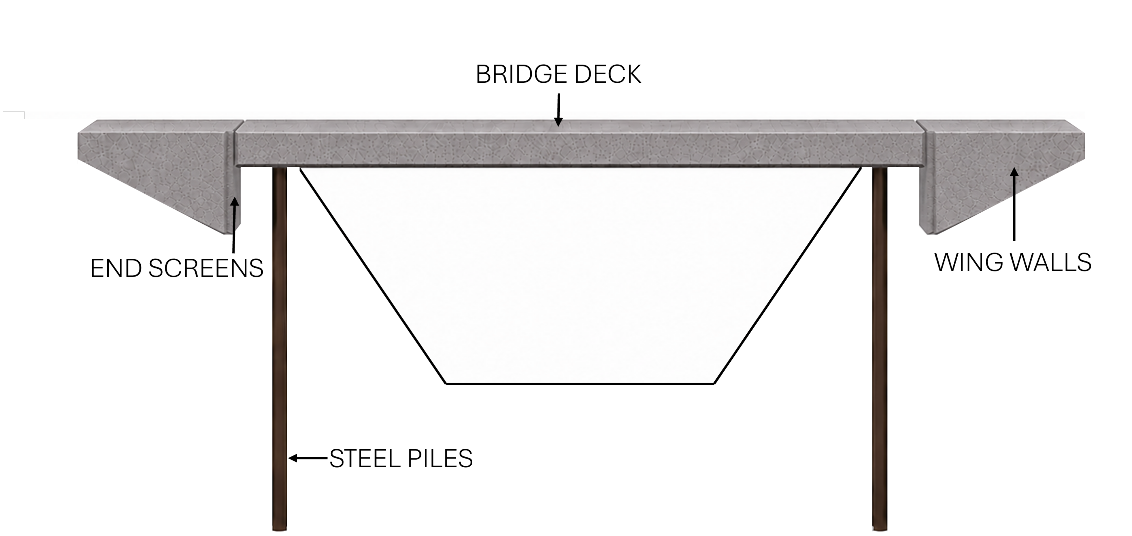

Figure 1.1: Conceptual sketch of an integral abutment bridge.

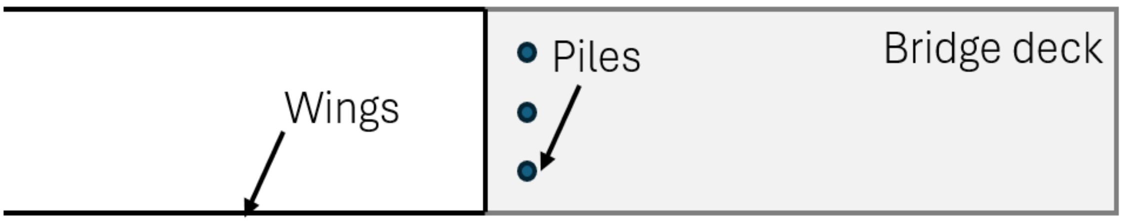

Figure 1.2: Conceptual sketch of a plan view of an integral abutment bridge with three piles.

1.2 Aim

The aim of this research is to investigate alternative design approaches of steel piles in integral abutment bridges. The purpose of the investigation is to estimate the structural capacity more realistically compared to the traditional design approach.

The study is based on a global buckling analysis of the system, including soil-structure interaction and steel piles cast into the superstructure. In BRIGADE/Plus a FE model is developed to capture the structural response. Ultimately, the objective is to develop a research-based comparison between the structural behaviour of a critical pile in the bridge system and a pile with a free or hinged pile head, which allows realistic design in the future.

1.3 Objectives

- To develop a FE model of an integral abutment bridge with steel piles.

- To investigate the global buckling behaviour of steel piles, including the influence of soil-structure interaction.
- To analyse reaction forces, bending moments, and load distribution within the bridge system.
- To compare the behaviour and capacity of the bridge system pile with corresponding single pile models under different boundary conditions.
- To assess which modelling assumption (free or hinged pile head) best represents the actual structural behaviour.

1.4 Limitations

This study is based on an integral abutment bridge with a maximum span length of 20 metres and a predefined geometry. The steel piles are assumed to consist of a standard structural steel grade commonly used in bridge design, and are modelled assuming steel-only sectional behaviour. This behaviour provides a conservative stiffness assumption, clearer interpretation of system-level effects, and reduced modelling uncertainty. In reality, the piles are often filled with concrete creating composite action. No corrosion is considered.

The analysis is performed using Design Approach 3 for all structural parts. Representative soil conditions are considered for sand and fine-grained soil with a constant unit weight and friction angle. The analysis excludes the upper layer of crushed material and instead the soil profile is modelled as a uniform soil type throughout the entire depth. Variations in soil properties, layering, and complex soil behaviour are not included in the scope.

Pile group effects are not considered in the single pile analyses or the corresponding hand calculations, since the piles are modelled as isolated structural elements. In the full bridge model, however, pile group interaction is included indirectly through the modelling of all six piles within the integrated bridge system, allowing interaction and force redistribution between the piles.

A full linear load combination analysis is not performed, instead the study is limited to a selected critical load case. The governing load case is assumed to be the vertical traffic load. All vertical and horizontal loads are applied to maximise the load effect on a specific pile.

1.5 Brief Research Methodology

This study applies a combination of literature review, case study, and FE modelling to investigate the behaviour of steel piles in integral abutment bridges. A literature review was conducted to establish a theoretical foundation for the study. Reports from relevant organisations, mainly the Swedish commission of pile research, and research on integral abutment bridges, pile design, and soil-structure interaction were reviewed.

Following the literature study, a case study of an existing bridge system was carried out to understand current practice. Design documents were used to examine geometry, structural components, and pile layout. The purpose of the case study was to identify how integral abutment bridges are analysed, including modelling assumptions, considering load effects, and simplifications.

The FEM-modelling was initiated using BRIGADE/Plus. The modelling process started with a simple model of a single pile to verify modelling approaches and ensure consistency with hand calculations. The model was gradually extended to include soil resistance, transverse loading, and different boundary conditions. In particular, the investigated boundary conditions in focus were free or hinged pile head. Hand calculations were performed in Mathcad Prime 11.0.1.0 and capacity graphs were created in Excel.

The critical pile in the bridge system and the single piles were then analysed to determine force, bending moment, and load distribution in two soil conditions. Based on the results, the applicability of different modelling assumptions was evaluated. The findings were used to develop recommendations for a more realistic and material efficient design approach.

1.6 Societal, ethical and ecological impacts

This study may contribute positively to society by establishing research-based guidelines that promote material-efficient design. Improved material utilization can lead to reduced construction costs while maintaining a robust and safe infrastructure, thereby supporting the sustainable development of bridge structures.

From an ethical perspective, civil engineers have a responsibility to balance safety and reliability with efficient use of resources. Transparent and well-founded decision-making is essential and the application of research-based design methods reduces the risk of arbitrary assumptions in engineering practice.

From an ecological perspective, reduced steel consumption directly contributes to lower CO_2 emissions. Therefore, material-efficient structural solutions have the potential to reduce the environmental impact of bridge construction and support the development of more sustainable infrastructure.

1.7 Use of AI

AI was used throughout this report for small grammar fixes to improve technical language. It was also used as a support tool to explain geotechnical and mathematical concepts and the behaviour of BRIGADE/Plus.

2

Literature study

This literature study presents relevant theory and current design practices related to integral abutment bridges. The reviewed theory covers the fundamental structural behaviour of this type of bridge, including soil-structure interaction, local and global buckling of piles, and commonly applied design methods. The literature review provides the theoretical basis for the FEM modelling phase and supports the evaluation of existing modelling approaches. By analysing current practices, the study aims to identify limitations and establish a foundation for the development of an improved modelling method for integral abutment bridges.

2.1 Integral abutment bridges

This chapter provides an overview of the structural behaviour of integral abutment bridges and the interaction between their main components. The bridge deck, abutments, piles, wing walls, and backfill act together as a continuous system, where vertical loads are primarily carried by the piles, while horizontal actions are resisted through a combination of pile bending and earth pressure acting on the end screens.

2.1.1 Concept and structural behaviour

An integral abutment bridge typically consists of a bridge deck, abutments formed by steel tubular piles filled with concrete and reinforcement, as well as wing walls and end screens installed to retain the backfill. The integral abutment bridge is a jointless bridge design, which means that the substructure is directly connected to the superstructure. This enables the abutment and superstructure to act as a single structural unit with rigid behaviour, ensuring full moment transfer (Ahn et al., 2011). It can be designed with different abutment configurations and foundation solutions. Common types include integral abutments founded on pad footings, pile supported integral abutments, and bank pad abutments. The following report will focus on the properties of an integral abutment bridge with a foundation of steel piles cast in the bridge deck.

Conventional bridges have expansion joints and bearings to respond to deformation and lateral load. By eliminating expansion joints and bearings, integral abutment bridges achieve a simpler structural system with reduced construction complexity.

This leads to improved durability and lower maintenance demands, as joints and bearings are common sources of degradation and water intrusion (Fennema et al., 2005).

Instead of transferring movement to bearings, integral abutment bridges transfer movement to the abutment-pile system, which depends on the soil-structure interaction and the stiffness of the system (Ahn et al., 2011). The stability of the bridge depends on the passive earth pressure acting on the abutment and the ability of the abutment piles to accommodate this movement. The uncertainties of seasonal temperature variations and internal restraint are a challenge with this type of bridges (Khodair & Hassiotis, 2005).

2.1.2 Interaction between superstructure and piles

The interaction between the superstructure and the piles is a fundamental aspect of integral abutment bridges. Due to the rigid connection, the loads and deformations are transferred directly between the superstructure and the piles without the presence of bearings or expansion joints. A simplified illustration of the connection is shown in Figure 2.1.

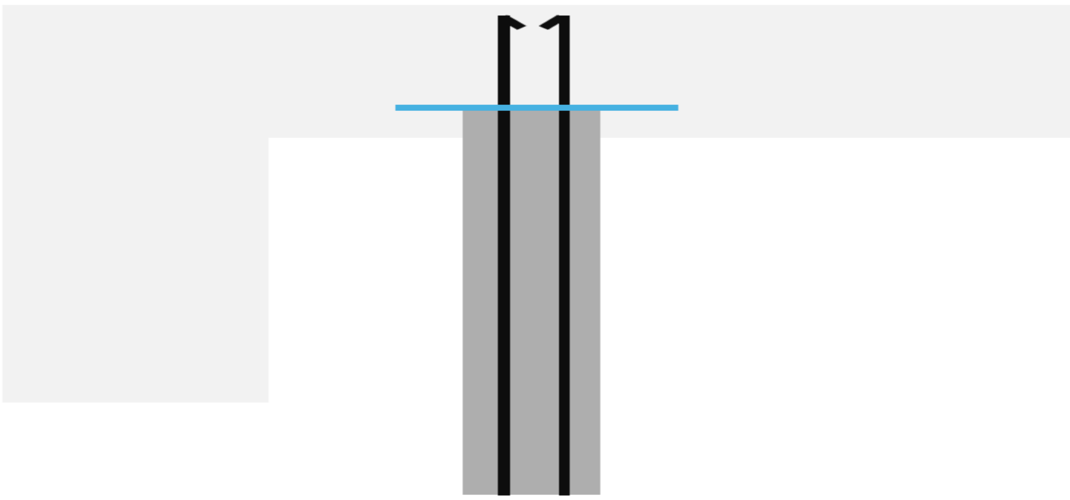

Figure 2.1: Sketch of a connection between the pile and the bridge deck.

The stiffness of the superstructure and the rigidity of the pile–deck connection influence the deformation compatibility between the bridge deck and the piles. A stiff superstructure restricts relative displacements and rotations at the pile head, affecting how forces and moments are distributed between the superstructure and the foundation. Consequently, the rotational behaviour at the pile head is not governed solely by the pile and surrounding soil, but also by the stiffness characteristics of the bridge deck and abutment structure. These interaction effects are essential for understanding the overall behaviour of integral abutment bridges and provide the basis for the stability considerations discussed in later sections.

2.1.3 Thermal movements and imposed deformations

Temperature changes affect the integral abutment bridges by causing expansion and contraction of the superstructure, forcing the bridge system to move towards and away from the surrounding backfill (Liu et al., 2022). At high temperatures, the bridge deck expands and the abutments are pushed against the backfill, leading to increased earth pressure. The opposite effects occur at low temperatures when the bridge deck contracts.

Temperature changes may lead to settlements in the backfill, cracks in the wing walls, and an increased bending moment in the pile foundation(Liu et al., 2022). For a bridge deck that is free to expand, the longitudinal length change, ΔL, is described as the product of the thermal expansion coefficient, α, the length of the bridge, L, and the temperature change, ΔT,

$$\Delta L = \alpha L \cdot \Delta T$$

However, an integral abutment bridge is not free to expand or contract due to the rigid connection between the bridge deck and the abutments (Liu et al., 2022). The bridge deck is restrained by the horizontal earth pressure and the stiffness of the piles, resulting in an actual length change that is smaller than the theoretical free expansion. Furthermore, the effective bridge deck temperature differs from the ambient air temperature and must be determined according to Eurokod 1: Laster på bärverk – Del 1-5: Temperaturpåverkan [SS-EN 1991-1-5], § 6.1.3.1, to ensure that realistic thermal loads are applied.

2.2 Soil-structure interaction

The behaviour of integral abutment bridges is strongly influenced by soil–structure interaction, where the response of the surrounding soil affects the distribution of forces and deformations within the bridge system.

2.2.1 Earth pressure theory for integral abutments

Different countries apply different approaches when considering horizontal earth pressures acting on integral abutments. In Germany, passive horizontal earth pressure is generally assumed behind the abutment, while design practices in Ireland and England consider earth pressures between the at-rest and passive states, depending on the magnitude of abutment movement. However, in Sweden, the additional horizontal earth pressure resulting from the abutment movement towards the backfill is taken into account (Liu et al., 2022).

The magnitude of the horizontal earth pressure behind an abutment is governed by the relationship between horizontal and vertical stresses in the soil. This relationship depends primarily on the ratio between the horizontal displacement of the top and the height of the abutment, as well as on the relative density of the backfill material. Larger abutment movements lead to increased mobilisation of the earth pressure (Liu et al., 2022). To predict the horizontal earth pressures acting on integral abutments, it is commonly assumed that the backfill soil mobilises passive earth pressure when the abutment moves towards the soil. This movement is caused by longitudinal actions such as braking loads or thermal expansion of the bridge deck. The mobilisation of passive earth pressure results in an increase in horizontal loads acting on the structure (Liu et al., 2022). According to (Trafikverket, 2011), it is assumed that the passive earth pressure is fully mobilised at a horizontal displacement corresponding to 1/200 of the height of the end screen. For displacement less than 1/200, the increase in earth pressure is determined by interpolation between the at-rest earth pressure and the passive earth pressure.

According to Pålkommissionen (2006, p. 20) the relationship between soil resistance and displacement is non-linear. At small stresses and displacements, the increase in earth pressure is approximately linear and lower than the maximum passive resistance that can be mobilised. However, for larger transverse loads and displacements, the soil response becomes non-linear. Therefore, it is important to account for the non-linear soil behaviour and the gradual mobilisation of passive earth pressure when analysing the interaction between soil and piles in integral abutment bridges.

During installation of displacement piles, the surrounding soil is also affected. In coarse-grained soils, pile driving generally leads to soil-densification, resulting in increased strength and stiffness. In fine-grained soils, pile installation initially alters the stress state around the pile, which may temporarily reduce the strength and deformation properties. Over time, as the soil-pile interaction develops, the soil tends to regain a portion of its original properties.

2.2.2 Soil modelling approaches for lateral pile support

There are several approaches to model soil behaviour in structural calculations. An approach is to assume that the soil behaves as a continuum with relevant mechanical properties. Another modelling approach is to model the soil-pile interaction as a beam laterally supported by an infinitely dense distribution of mutually independent springs. The surrounding soil is represented by springs that provide resistance when the pile is exposed to transverse loading. Spring stiffness may vary depending on the properties of the local soil it represents. This approach is referred to as the Winkler method or the use of "p-y" curves (Pålkommissionen, 2000).

Soil behaviour is generally described using an elastic-plastic model. When geometric non-linearities and second-order effects are considered, and in some cases cyclic or dynamic loading, numerical methods are required to enable gradual loading and accurately represent the soil-structure interaction (Pålkommissionen, 2006). However, models are complex, and the choice of modelling approach represents a compromise between theoretical accuracy and practical applicability.

2.3 Pile behaviour and stability

This chapter addresses the stability of piles in integral abutment bridges, with particular focus on buckling behaviour. The influence of initial pile imperfections is first discussed, followed by the effect of soil-pile interaction and its depth-dependent behaviour. The final part of the chapter compares local and global analysis approaches and illustrates how different modelling assumptions may lead to different stability assessments. System-level boundary conditions are discussed to provide a basis for evaluating pile stability under combined loading.

2.3.1 Initial imperfections in piles

Initial imperfections have a significant influence on the stability behaviour of slender piles. In practice, piles are never perfectly straight or perfectly aligned after installation. Geometrical imperfections, such as initial curvature, construction tolerances, and introduction of eccentric load, create initial bending moments in the pile.

For piles subjected to high axial loads, these imperfections become particularly important since deformations can be amplified by second-order effects (Pålkommissionen, 2006). The interaction between axial force and lateral displacement reduces the effective load-carrying and buckling capacity compared to an ideal, perfectly straight pile. Consideration of initial imperfections is therefore necessary to obtain realistic predictions of pile behaviour and stability.

2.3.2 Buckling behaviour of piles in soil

The buckling behaviour of piles embedded in soil differs from the classical Euler buckling of free-standing columns. The surrounding soil provides continuous lateral support along the length of the pile, which restrains lateral deformations and increases the critical buckling load. As a result, the effective buckling length becomes shorter than the unsupported pile length.

The stability behaviour of the piles is therefore governed by the interaction between pile stiffness, axial force, and the lateral restraint provided by the surrounding soil (Pålkommissionen, 2006). Since the lateral soil support varies with the soil conditions and depth, the buckling mode and deformation shape of the embedded piles differ from those of unsupported columns.

2.3.3 Global vs local buckling

Pile design in integral abutment bridges is commonly based on local analyses, where a single pile is studied independently of the surrounding structural system. In such models, the pile is typically assumed to be fixed at the pile toe and free to rotate and translate laterally at the pile head. The buckling capacity is then governed by the pile geometry, material properties, assumed boundary conditions, and the lateral support provided by the surrounding soil.

When the pile head is assumed to be free, the effective buckling length becomes relatively large, resulting in a lower critical buckling load. Local pile analyses therefore often lead to conservative estimates of pile stability.

In contrast, global buckling considers the stability of the entire bridge foundation system. In a global analysis, the bridge deck, abutments, wing walls, and piles are modelled together as an interacting structural system. The stiffness of the superstructure restricts rotations and lateral displacements at the pile head, resulting in a shorter effective buckling length and an increased critical buckling load compared to a local pile analysis.

2.3.4 Composite action and stiffness contribution

Steel piles filled with concrete are often used in integral abutment bridges due to the benefits of the composite action. It increases bending stiffness near the pile head, and improves durability and constructibility when casting into the abutment. To fully utilise the contribution of the concrete, a full interaction between the steel pipe, the concrete, and the ground is required, this interaction must already be activated at the pile head (Pålkommissionen, 2018).

The increased stiffness of the composite action will reduce the curvature of the pile and second-order effects, and the buckling resistance will also increase. Due to cyclic thermal movements of the bridge deck, the piles are subjected to alternating bending directions, which may lead to cracking of the concrete core.

Piles are often modelled assuming steel-only sectional behaviour. The composite action of concrete is neglected in the initial modelling phase. Steel-only behaviour provides a conservative stiffness assumption, a clearer interpretation of system-level effects, and reduced modelling uncertainty.

2.4 Loads and load combinations

Loads can be classified as permanent or variable actions. These loads act in the vertical, longitudinal, or transverse direction. Figure 2.1 presents the relevant loads considered in this study, their direction of action, and their primary effects on an integral abutment bridge. The following sections describe in more detail the effects of vertical and horizontal loading.

Table 2.1: Permanent and variable loads, how they act and the most critical effects.

Permanent loads	**Load direction**	**Primary structural effect**
Self weight	Vertical	Bending moments in piles and bridge deck.
Coating	Vertical	Bending moments in piles and bridge deck.
Earth Pressure	Horizontal	Contributes to lateral restraint and stability of the abutment system.
Shrinkage	Longitudinal	Contraction of the bridge deck and additional restraint forces.
Variable loads	**Load direction**	**Primary structural effect**
Distributed traffic load	Vertical	Bending moments in piles and bridge deck. Axial force in pile.
Axle traffic load	Vertical	Bending moments in piles and bridge deck. Axial force in pile.
Braking and acceleration loads	Longitudinal	Bending moments in piles and end screens.
Lateral traffic load	Transverse	Bending moments in piles.
Wind	Primarily transverse	Transverse loading and uplift effects on the bridge structure.
Surcharge	Horizontal	Increases the horizontal earth pressure acting on the abutments.
Thermal effects	Longitudinal	Causes thermal expansion, contraction and restraint forces in the bridge deck.

2.4.1 Vertical loads

Vertical loads in integral abutment bridges consist primarily of permanent loads, such as self-weight and surfacing loads, together with variable traffic loads according to Eurokod 1: Laster på bärverk – Del 2: Trafiklaster på broar [SS-EN 1991-2]. The primary load-carrying system for vertical loading is the piles, where vertical actions mainly contribute to axial compressive force. In slender piles, the magnitude of the axial force becomes particularly important because it influences the stability behaviour and the sensitivity to buckling.

Although vertical loads primarily generate axial forces, bending moments may arise due to horizontal actions, imposed deformations, and initial imperfections. The presence of axial force amplifies these bending effects through second-order behaviour. The interaction between axial force and bending moments is therefore decisive for the buckling resistance of the piles (Pålkommissionen, 2000).

Traffic loads are commonly represented using Load Models 1, 2 and 3 according to SS-EN 1991-2, consisting of distributed lane loads and concentrated axle loads. Depending on the load position, the traffic load can contribute to an uneven force distribution between the piles and increased axial forces in the critical outer piles.

2.4.2 Horizontal loads and imposed deformations

Temperature actions generate imposed deformation rather than directly applied force. Due to the integral connection between the superstructure and the abutments, longitudinal movements are restrained by the surrounding structural system and soil. This restraint leads to mobilisation of the earth pressure acting on the end screens. Horizontal forces are transferred through the integral abutment into the pile rows, where they are resisted primarily by pile bending and soil-structure interaction. These effects are particularly important in integral abutment bridges due to the absence of expansion joints and bearings.

Braking forces constitute horizontal loads applied directly acting in the longitudinal direction of the bridge. These forces are transferred through the deck to the end screens and further into the piles. In the transverse direction, horizontal actions, such as wind loads and vehicle impact, are primarily resisted by the wing walls. The wing walls act as load-collecting elements and transfer horizontal forces into the pile foundation system.

In the structural system, the interaction between piles, end screens, and wing walls is governed by displacement compatibility and relative stiffness. In numerical analysis, the load distribution depends on the horizontal stiffness in the construction elements.

The piles resist horizontal loads primarily through bending, where the lateral response is governed by the interaction between the stiffness of the bending of the pile and the surrounding soil along the length of the pile. In the adopted modelling assumptions, the backfill soil behind the end screens restrains longitudinal displacements of the superstructure, but does not contribute directly to the lateral stabilisation of the piles themselves.

2.4.3 Load combinations relevant for stability

The stability of piles in integral abutment bridges is governed by the interaction between axial force and bending moments. The maximum axial force and the bending moment do not necessarily occur simultaneously, as they originate from different load effects. Vertical loads primarily generate axial force, while horizontal actions and imposed deformations generate bending moments. Consequently, several load combinations must be evaluated to identify the governing load case for pile stability.

In the Ultimate Limit State (ULS), the piles are verified against collapse, loss of stability and structural failure in accordance with Eurocode – Basis of structural design [SS-EN 1990]. Relevant ULS combinations for pile stability consist of vertical loads acting simultaneously with horizontal actions or imposed deformations, resulting in combined axial force and bending moments. These combinations are critical due to second-order effects, where axial force amplifies bending moments and lateral deformations.

In the Serviceability Limit State (SLS), piles are verified with respect to deformations, displacements, and long-term effects. Although SLS does not govern ultimate capacity, serviceability load combinations may still generate significant horizontal displacement and bending moments caused by temperature effects, shrinkage and sustained loads. These deformations influence the stability behaviour by increasing the sensitivity to second-order effects and are therefore relevant when assessing pile stability in integral abutment bridges.

3

Numerical model

This chapter presents the numerical modelling approach used to evaluate the structural behaviour of integral abutment bridge piles subjected to combined axial and lateral loading. The FE-modelling was performed in BRIGADE/Plus and includes the modelling assumptions, material properties, soil conditions, applied loads, and verification procedures adopted throughout the study.

The modelling process was developed progressively, starting with simplified single pile models used for verification and sensitivity analyses, before extending the approach to a full bridge system including soil-structure interaction and geometric non-linearity. Two different soil conditions were analysed to evaluate the influence of soil stiffness on pile behaviour and redistribution mechanisms.

The chapter also describes the implementation of loads, boundary conditions, and numerical procedures used to capture instability behaviour, plastic hinge formation, and redistribution of internal forces within the bridge system.

3.1 Soil characteristics

The bridge structure are evaluated with two different types of soil. The first soil is assumed to be homogeneous coarse grained soil with a constant unit weight and internal friction angle. The simplification with constant parameters was made to adapt the study to the project time frame and to reduce model complexity. However, the limit pressure in the sand increases with depth due to the increase in effective vertical stress with depth. The second soil is fine-grained soil with a constant shear modulus. The end screens and the wing walls are embedded in dense backfill. All soil properties are presented in Table 3.1 together with the geometry and material properties.

To evaluate the influence of the surrounding soil on the bridge system and the steel piles, soil-related parameters were calculated. Limit pressures and their corresponding depths were computed in Mathcad, Appendix A, and later implemented in the FE model. The interaction between soil and piles was modelled in BRIGADE/Plus using p–y-curves to represent the non-linear and plastic behaviour of the soil. The soil stiffness was defined by springs distributed along the length of the pile according to a Winkler foundation model, as described in Section 2.2.2.

The same modelling approach with a p-y-curve was used for the end screens and wing walls. The passive earth pressure was assumed to be fully mobilised when the horizontal displacement towards the soil reached 1/200 of the height of the retaining wall, according to Trafikverket, 2011.

3.2 Model input and loading

This chapter describes the input data, summarised in Table 3.1, and loading conditions used in the numerical analyses. The model is defined by the geometric configuration, the properties of the material, and the soil parameters, together with the load cases required to represent the governing actions on the structure.

3.2.1 Input parameters

The reference bridge in the case study provides the geometric basis for the integral abutment bridge analysed throughout this study. The bridge geometry remains unchanged during the hand calculation phase and the FE modelling.

The steel piles and the bridge deck are modelled using commonly applied grades of structural steel and concrete. A design service life of 120 years is adopted based on current bridge design practice.

Table 3.1: Table of input data.

Geometry		**Steel**		**Concrete**	
Span length	20 m	Steel grade	S460	Concrete Class	C35/45
Pile diameter	0.32 m	Density	7850 kg/m^3	Density	2500 kg/m^3
Pile length	20 m	Youngs modulus	210 GPa	Youngs modulus	34 GPa
		Poissons ratio	0.3	Poissons ratio	0.2
Sand		**Fine-grained soil**		**Backfill**	
Type	Sand	Subgrade modulus	20 kPa	Unit weight	22 kg/m^3
Friction angle	34°	Permanent load	50 %		
Unit weight	18 kg/m^3				

3.2.2 Load definitions

All loads were positioned on the bridge system to produce the most unfavourable loading condition for a single pile, presented in Figure 3.1. The combination of applied loads consisted of permanent and variable actions. The dead weight were determined directly by BRIGADE/Plus based on the density of the material, gravitational acceleration, and dimensions of the bridge.

Several temperature load cases were evaluated through combinations of thermal contraction, thermal expansion, and temperature gradients within the bridge deck,

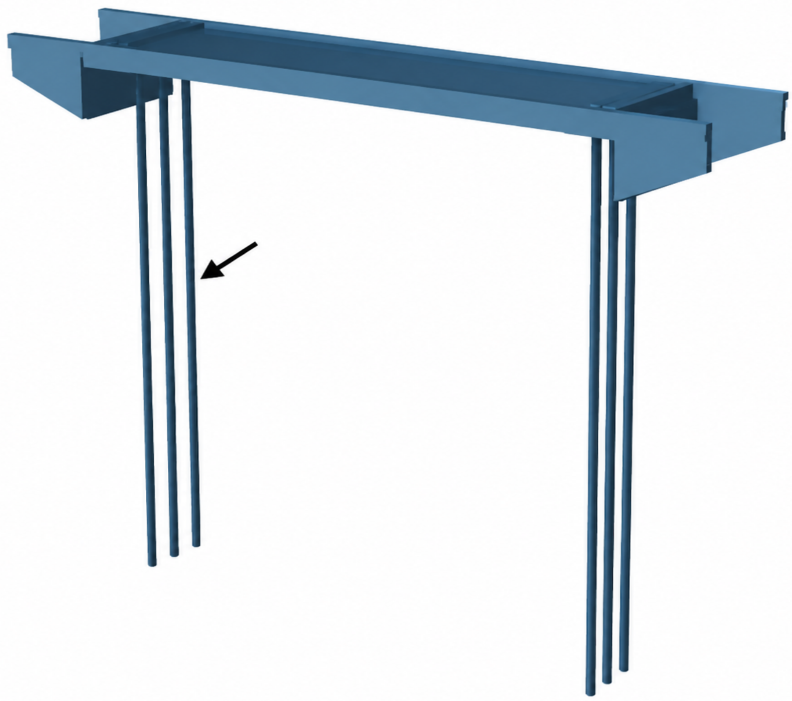

Figure 3.1: Bridge system with the pile subjected to the highest load effects marked.

where the upper side of the deck was warmer or colder than the lower side. The most unfavourable combination was found to be thermal contraction combined with a warmer lower side of the deck. This load case increased the curvature of the bridge deck and generated larger bending moments in the piles. The relevant temperature load cases are presented in Appendix B.

The wind load was applied on the same side as the critical pile, acting on the wing walls and the edge beams. This load configuration created an uplifting effect on the bridge structure, which increased the tensile forces in the outer pile.

Traffic loads were applied according to SS-EN 1991-2, where Load Model 1 (LM1) was adopted. To create the most unfavourable load position, the distributed traffic load was placed directly above the pile on one side of the traffic lanes. The braking force was applied longitudinally to the traffic lanes, while the lateral load was applied perpendicularly to the edge beam. The surcharge load was positioned on the end screen farther away from the critical pile, in the same direction as the braking force. These horizontal loads generated additional bending moments in the integral abutment system and contributed to increased pile forces. The effect of each load, on the critical pile, is shown in Figure 3.2 together with LM1. The graph illustrates whether the applied loads govern the bending moment and the normal force.

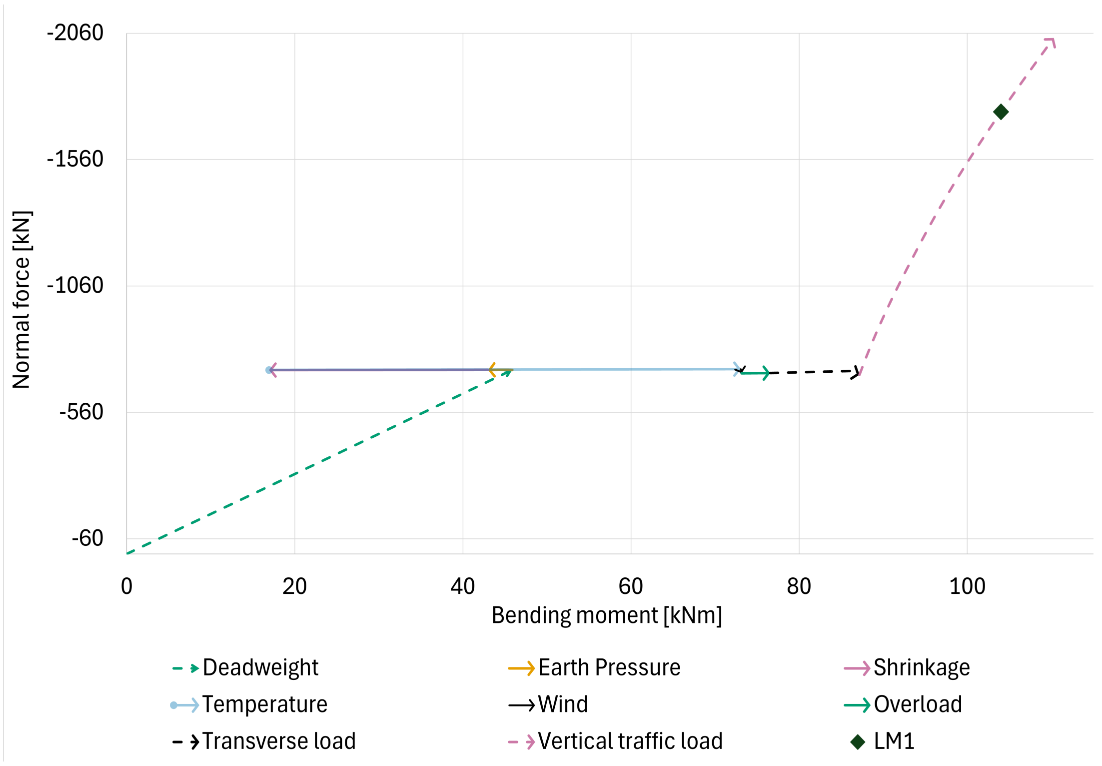

Figure 3.2: LM1 and the applied loads, showing their influence on the critical pile's bending moment and normal force.

3.3 BRIGADE/Plus setup

The FEM-modelling was initiated using BRIGADE/Plus. The modelling process started with a simple model of a single pile to verify modelling approaches and ensure consistency with hand calculations. The model was gradually extended to include soil resistance, transverse loading, and different boundary conditions. In particular, the investigated boundary conditions in focus were free and hinged pile head and the pile toe fixed and restrained from torsion.

After verifying the modelling approach, a full-scale model of the bridge system was developed in BRIGADE/Plus. The model included soil-structure interaction and piles cast into the superstructure to allow integrated structural behaviour. The connection between the bridge deck and the piles was defined such that the deck acts as the primary structural component and the pile heads are treated as secondary nodes. This configuration restrains the pile heads through the superstructure, while the pile bases are fixed in all translational directions, but remain free to rotate. A predicted worst load combination was applied to the bridge system, based on the assumptions described in Section 1.4.

The piles and the edge beams were modelled as beam elements, while the bridge deck, wing walls and end screens were modelled as shell elements with a structured quadrilateral mesh. The shell elements were assigned a global mesh size, ensuring sufficient resolution to capture the bending behaviour in the superstructure, presented in Table 3.2.

Geometric non-linearity was included to capture large displacement effects, and the analysis was performed using a static procedure with a controlled increment size appropriate to the job. The formation of plastic hinges and moment redistribution were monitored through element output of bending moments, curvatures, and plastic strains. The loads were applied in BRIGADE/Plus according to the load definitions presented in Section 3.2.2. To allow load accumulation, step type ”Static, General” and ”Static, Riks” were applied. All selections regarding load application are summarised in Table 3.3.

To account for the bending moment generated in the pile by the self weight of the bridge deck in the full bridge system model, an equivalent bending moment was applied at the pile head in the single pile analyses. This ensures that the single pile models start from the same moment state as the pile in the bridge system, prior to additional loading.

The influence of soil stiffness and boundary conditions was evaluated to assess the structural behaviour of the system. Based on the results, the applicability of different modelling assumptions was evaluated, including free and laterally supported pile heads. The findings were used to draw conclusions from the study and determine the most realistic design approach.

Table 3.2: BRIGADE/Plus modelling choices.

Element	Element type	Mesh size	Mesh form
Bridge deck, end screens, wing walls	First-order shell (S4R)	0.35 m	Quadrilateral
Piles, edge beams	First-order beam (B31)	-	-

Table 3.3: BRIGADE/Plus steps and loading.

Step	Load	Unit	NLGEOM	Step type
Initial	-	-	N/A	(Initial)
Dead weight	Dead weight, coating	N/m^2	ON	Static, General
Earth pressure	Earth pressure	N/m^2	ON	Static, General
Shrinkage	Shrinkage	K	ON	Static, General
Temperature	Temperature difference for contraction	K	ON	Static, General
Temperature difference	Lower side warmer than upper side	K	ON	Static, General
Wind	Wind load wing walls, wind load edge beam	N/m^2	ON	Static, General
Surcharge	Surcharge	N/m^2	ON	Static, General
Braking/Acceleration	Braking/Accelation load	N	ON	Static, General
Lateral load	Lateral load	N	ON	Static, General
Vertical traffic load	Axle load, distributed traffic load	N, N/m^2	ON	Static, Riks

3.4 Verifications and sensitivity analysis

A sensitivity analysis and verification procedures were carried out, to ensure the reliability of the study and set up of the FE model. The FE model was compared to hand calculations to assess differences in forces, bending moments, and pile capacity. Reduction factors were set to 1.0 in the hand calculations to ensure consistency with the modelling assumptions used in BRIGADE/Plus. All hand calculations are presented in Appendices A to E. The sign convention follows structural engineering.

3.4.1 Single pile

The verification process started with a simplified model of a single pile subjected to an axial load without soil resistance. The hand calculations (HC) were compared with the numerical model to confirm consistency. In the next step, elastic and elastic-plastic soil resistance was added to study the effect of soil-structure interaction. The pile has always an elastic-plastic material response in BRIGADE/Plus.

After validating the simple cases, the single pile was analysed under two different boundary conditions: one case with a free pile head subjected to axial and transverse loads, and one case with a hinged pile head subjected to axial load only. Both cases were tested with elastic and linear elastic perfectly plastic soil response.

A sensitivity analysis was performed by varying the stiffness of the surrounding soil. The results of the analysis of a laterally supported pile are presented in Figure 3.3 and Figure 3.4. Figure 3.3 shows the normal force and displacement of the pile for the elastic and elastic-plastic response of the soil. The axial capacity is lower with elastic-plastic response, which shows the impact of yield in the soil. Figure 3.4 presents the normal force and bending moment in the pile, the interaction curve is based on material characteristics of the pile. The results indicate that for very stiff soil conditions, the pile reaches material failure. For lower soil stiffness, for example $k_d d$ = 500 kN/m/m, the curve deviates before reaching the interaction line, indicating instability failure. The indication of plastic behaviour determined in Appendix C is marked in Figure 3.4 .

The differing results from BRIGADE/Plus and the hand calculations indicate that the hand-calculated approach is more conservative than the numerical analysis. In the hand calculations, the pile response is assumed to remain linear until the soil begins to yield, after which the pile capacity drops, leading to a quick failure. In contrast, the numerical analysis shows that the pile can mobilize additional capacity, allowing the load to redistribute within the pile and sustain higher forces for a longer duration.

Table 3.4 summarises the input parameters used in the verification of the single-pile models, including variations in soil stiffness, soil response, and the initial imperfection, δ, applied in each analysis.

Table 3.4: Modelling data for verification of a single pile.

Restrained pile head, subjected to vertical load			
	$k_d d$ [kN/m^2]	Soil response [MPa]	δ[mm]
5500 E	5500	Elastic	22.3
5500 EP	5500	Elastic–Plastic	22.3
HC 5500 EP	5500	Elastic–Plastic	22.3
3000 E	3000	Elastic	25.9
3000 EP	3000	Elastic–Plastic	25.9
HC 3000 EP	3000	Elastic–Plastic	25.9
1000 E	1000	Elastic	34.1
1000 EP	1000	Elastic–Plastic	34.1
HC 1000 EP	1000	Elastic–Plastic	34.1
500 E	500	Elastic	40.5
500 EP	500	Elastic–Plastic	40.5
HC 500 EP	500	Elastic–Plastic	40.5
Free pile head, subjected to vertical and transverse load			
	$k_d d$ [kN/m^2]	Soil response [MPa]	δ[mm]
5500 E	5500	Elastic	22.3
5500 EP	5500	Elastic–Plastic	22.3
3000 E	3000	Elastic	25.9
3000 EP	3000	Elastic–Plastic	25.9
1000 E	1000	Elastic	34.1
1000 EP	1000	Elastic–Plastic	34.1
500 E	500	Elastic	40.5
500 EP	500	Elastic–Plastic	40.5

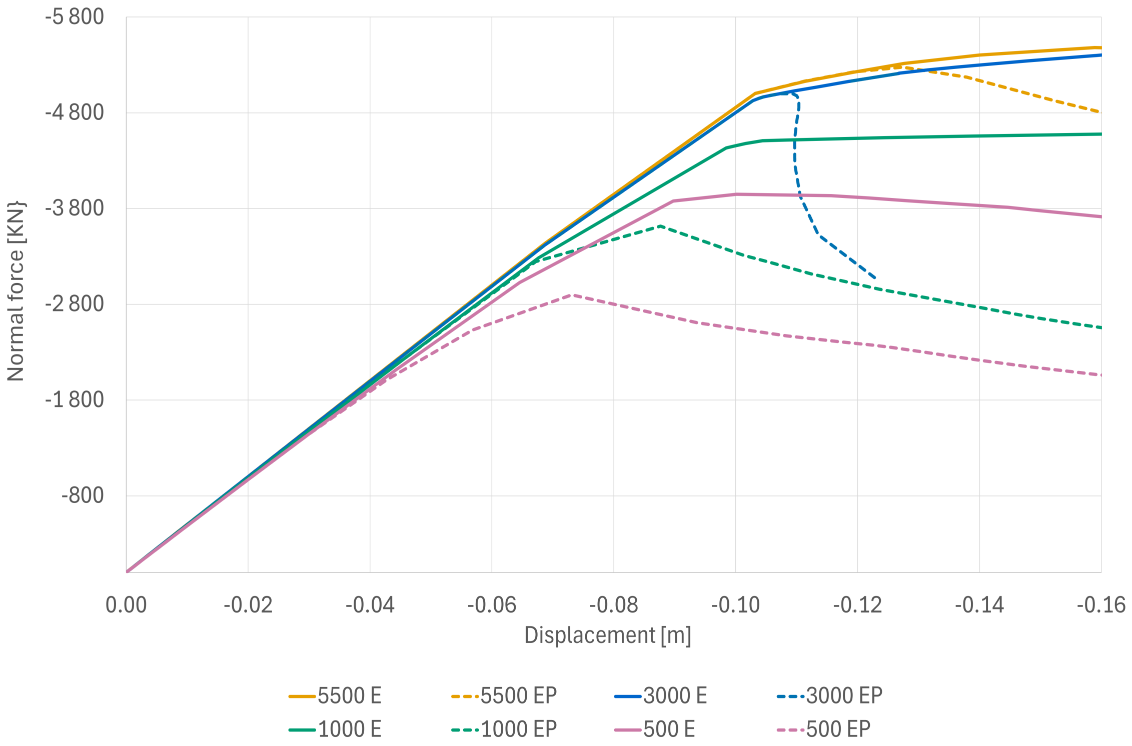

Figure 3.3: The correlation of normal force and deflection for piles surrounded by elastic (E) and elastic-plastic (EP) soil.

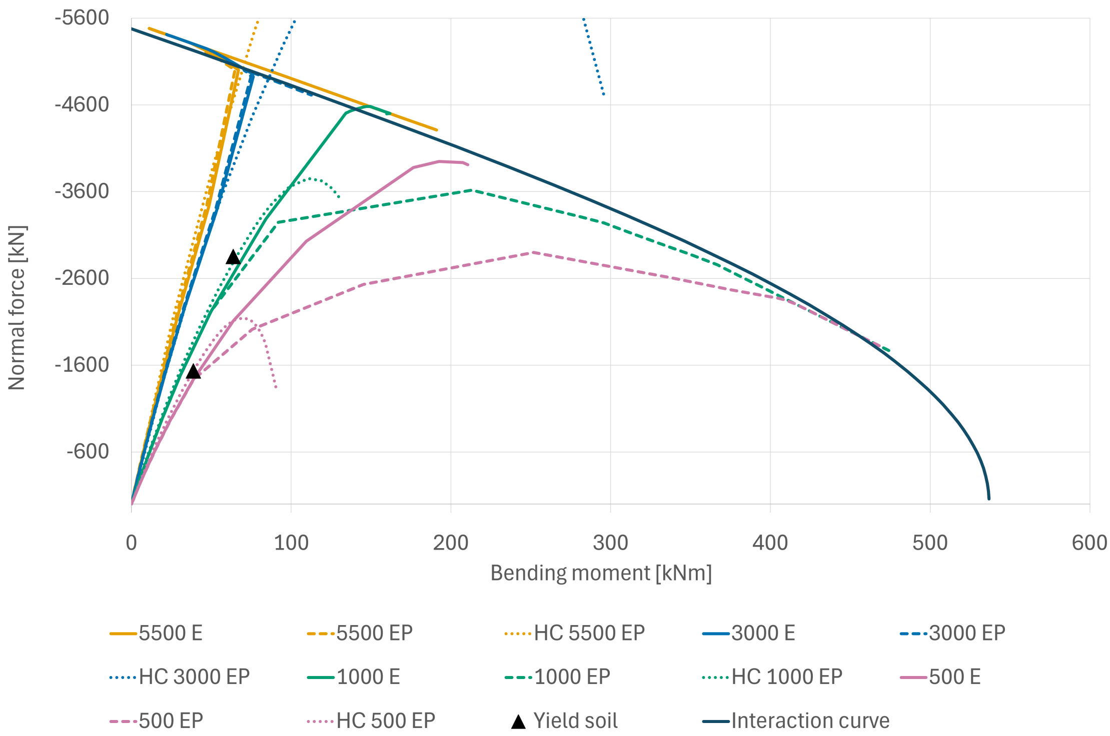

Figure 3.4: The correlation of normal force and bending moment for piles surrounded by elastic (E) and elastic-plastic (EP) soil. Interaction curve included.

The same sensitivity analysis was performed for the free pile head loaded with axial force and transverse load, presented in Figures 3.5 and 3.6. Only BRIGADE/Plus results are included in the graphs, as hand calculations do not cover the full capacity of the pile. In Appendix D the calculations for the bending moment due to transverse load are presented. In BRIGADE/Plus the pile were first loaded with the transverse load and then with the axial load. Both figures show that the soil starts to yield during the transverse loading for a lower soil stiffness.

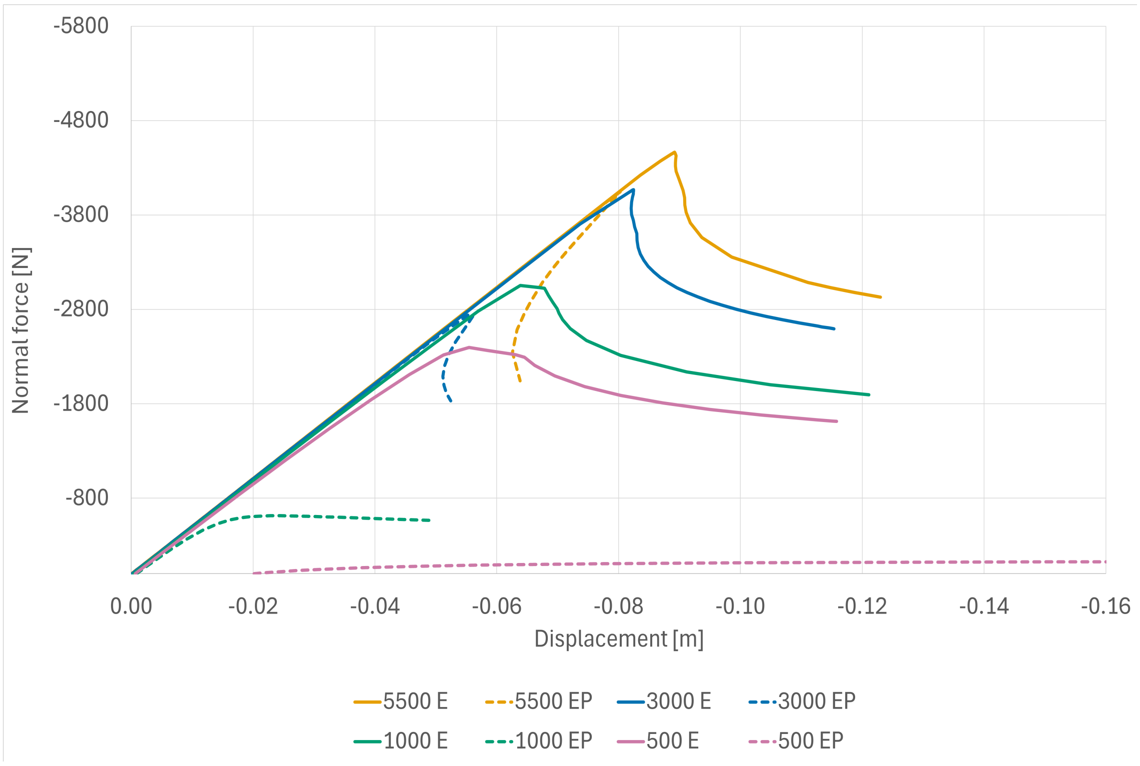

Figure 3.5: The correlation of normal force and deflection for piles surrounded by elastic and elastic-plastic soil.

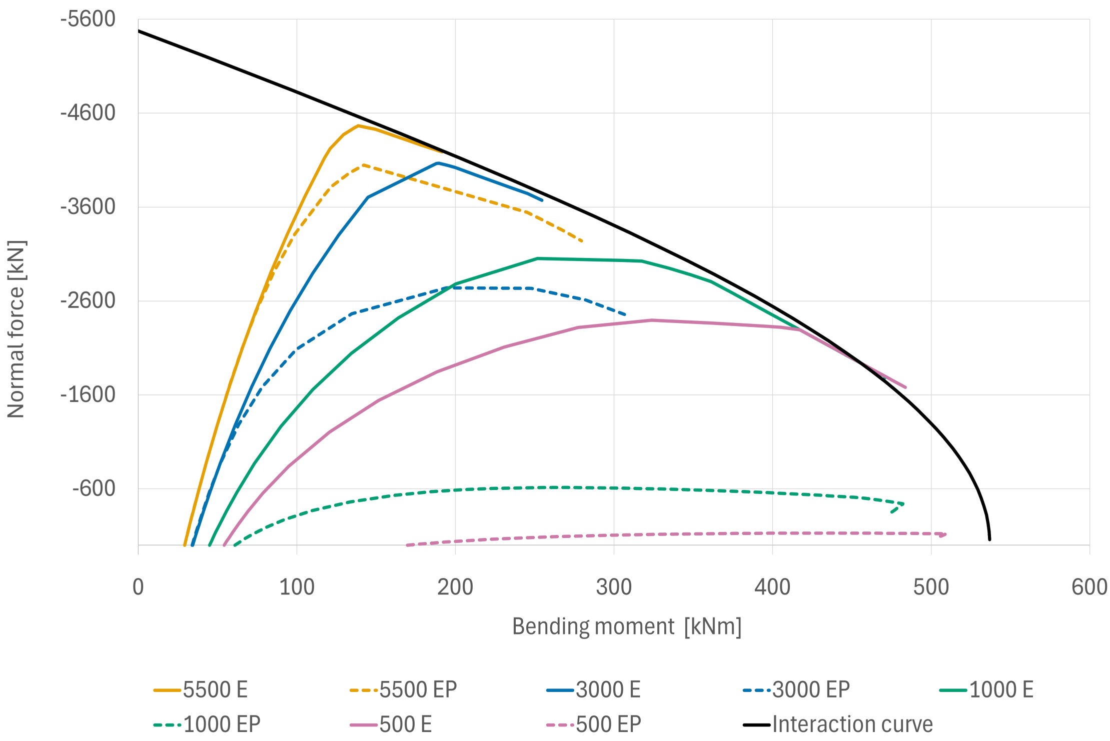

Figure 3.6: The correlation of normal force and bending moment for piles surrounded by elastic and elastic-plastic soil. Interaction curve included.

3.4.2 Buckling mode identification

The buckling behaviour was verified using a single pile model. A vertical reference load was applied to the pile to identify the governing buckling direction, to which horizontal loads were applied in subsequent analyses. The buckling behaviour, together with initial imperfections, illustrated realistic buckling modes including second order effects.

The buckling analysis in BRIGADE/Plus provides an eigenvalue that represents a load multiplier applied to the reference load. Critical sectional forces can therefore be approximated by multiplying the obtained finite element-force by the eigenvalue factor. In the single pile model, it was possible to directly compare the theoretical critical buckling load with the Brigade eigenvalue factor since the pile was subjected to a reference load of 1 N.

The theoretical normal force for a free pile head is determined by: (Pålkommissionen, 2006)

$$P_k = 2\sqrt{k_d d \cdot E \cdot I}$$

and for a hinged pile head:

$$P_k = \sqrt{k_d d \cdot E \cdot I}$$

3.4.3 Verification of the full bridge system

Verifications were performed on the complete bridge system model to ensure realistic structural behaviour. A horizontal point load of 100 kN was applied in the centre of the end screen to study the deformation patterns and the load distribution. For the sand case, this loading resulted in approximately 60% of the horizontal force being carried by the end screens. The structure was also analysed under self-weight only, to verify the expected deformation behaviour. This method ensures a realistic distribution of horizontal forces within the system.

To further evaluate correct modelling of the springs, soil resistance was deactivated for piles and abutments in separate analyses. When soil resistance is neglected for the piles, a larger portion of the load is transferred to the abutments, and vice versa.

The influence of temperature was evaluated to determine the governing case. A temperature decrease was found to be the most unfavourable condition for the structure and was therefore used in the critical load combination.

Table 3.5 summarises the input data used in the analyses of the full bridge system, including the considered load cases, applied additional moments (M) and axial loads (N), together with the initial imperfections (δ). The corresponding results are presented in Chapter 4.

Table 3.5: Modelling data for verification of the full bridge system.

Stiff sand				
Case	**Explanation of pile/cross-section**	M **[kNm]**	N **[kN]**	δ **[mm]**
Critical pile	In full bridge system	–	–	22.3
Restrained, 1	Restrained pile head, max. bending under LM1	46.0	–	22.3
Restrained, 2	Restrained pile head, max. bending at failure	46.0	–	22.3
Free, 1	Free pile head, max. bending under LM1	46.0	58.3	22.3
Free, 2	Free pile head, max. bending at failure	46.0	58.3	22.3
Cross-section 1	Section where 1st plastic hinge forms	46.0	–	22.3
Cross-section 2	Section where 2nd plastic hinge forms	46.0	–	22.3
Cross-section 3	Section where 3rd plastic hinge forms	46.0	58.3	22.3
Cross-section 4	Section where 4th plastic hinge forms	46.0	58.3	22.3
Fine-grained soil				
Critical pile	In full bridge system	–	–	22.3
Restrained, 1	Restrained pile head, max. bending under LM1	29.6	–	22.3
Restrained, 2	Restrained pile head, max. bending at failure	29.6	–	22.3
Free, 1	Free pile head, max. bending under LM1	29.6	21.6	22.3
Free, 2	Free pile head, max. bending at failure	29.6	21.6	22.3
Cross-section 1	Section where 1st plastic hinge forms	29.6	–	22.3
Cross-section 2	Section where 2nd plastic hinge forms	29.6	–	22.3
Cross-section 3	Section where 3rd plastic hinge forms	29.6	21.6	22.3
Cross-section 4	Section where 4th plastic hinge forms	29.6	21.6	22.3

4

Results

This chapter presents the results of the study. The single pile with free and hinged pile head, and the critical pile within the bridge system are compared in two soil conditions to ensure more robust and nuanced results. The first case consists of stiff sand, while the second case consists of fine-grained soil that represent a weaker soil profile.

The results are presented in graphs and tables that illustrates force distribution, bending moments, structural response, and ultimate capacity. For the full bridge system model, the development of plastic hinges and redistribution of internal forces are also presented.

4.1 Maximum normal force capacity

The maximum axial load capacity for each case is summarised in Table 4.1. For each configuration, the table presents the axial load level in the pile at which soil yielding and steel yielding occur, providing an overview of the governing mechanisms that limit the capacity in each case.

In the free pile head cases, yielding of the soil first occurs near the ground surface because of the deflection from the horizontal forces. This reduces the lateral support provided by the surrounding soil, but the steel pile is still able to sustain additional axial load. Failure occurs when yielding develops in the steel pile and the pile loses stability.

For the restrained pile head configurations, simultaneous formation of plastic hinges occurs at multiple locations along the pile. Plastic hinges may develop in the steel while the pile is still able to sustain additional vertical loading. However, once plastic behaviour also develops in the surrounding soil, failure occurs shortly thereafter due to the reduced stabilising effect of the soil support.

The pile in the studied bridge system, in fine-grained soil, shows behaviour similar to the single pile cases, where failure occurs once yielding has developed in both the steel pile and the surrounding soil. In the sand case, the surrounding soil remains stiff enough to provide lateral support throughout the loading process. Instead of soil failure governing the response, plastic hinges gradually develop along the steel pile until most of the pile section has yielded, after which failure occurs.

Table 4.1: Summary of results for the analysed pile cases. The axial force when the critical pile fails, the soil yields and the steel yields is presented.

Sand	N_{max}[kN]	$N_{y.soil}$[kN]	$N_{y.steel}$[kN]
Free pile head	3254	1980	3255
Restrained pile	5190	5166	4940
Critical pile in bridge	5480	-	3958
Fine-grained soil	N_{max}[kN]	$N_{y.soil}$[kN]	$N_{y.steel}$[kN]
Free pile head	2718	2411	2718
Restrained pile	4340	4341	3936
Critical pile in bridge	4605	4618	4045

4.2 Evaluation of pile behaviour in stiff sand

Figures 4.1 and 4.2 present the response of a single pile with a free and hinged pile head, as well as the critical pile in the bridge system in stiff sand. In Figure 4.1, it is shown that the normal force increases with deflection until the pile reaches its maximum capacity. After this point, the normal force decreases while the deflection continues to increase. As shown in the graph, the pile within the bridge system exhibits a normal force capacity marginally greater than that of the single pile with a hinged pile head.

The location of the maximum bending moment changes as the vertical load increases. Therefore, the correlation between normal force and bending moment in the single pile cases is presented from two cross-sections in Figure 4.2: the section with maximum bending moment under LM1 loading, named "Free , 1" and "Restrained, 1", and the section with maximum bending moment at failure, "Free, 2" and "Restrained, 2". Since neither the single pile nor the bridge system pile buckles purely in x or y-directions, the bending moment from both axes is included. Also, the point where soil and steel yield is marked in the graph. For the critical pile in the bridge system, the maximum bending moment consistently occurs at the pile head. The results show that the capacity reaches the interaction curve, indicating that material failure occurs before instability failure.

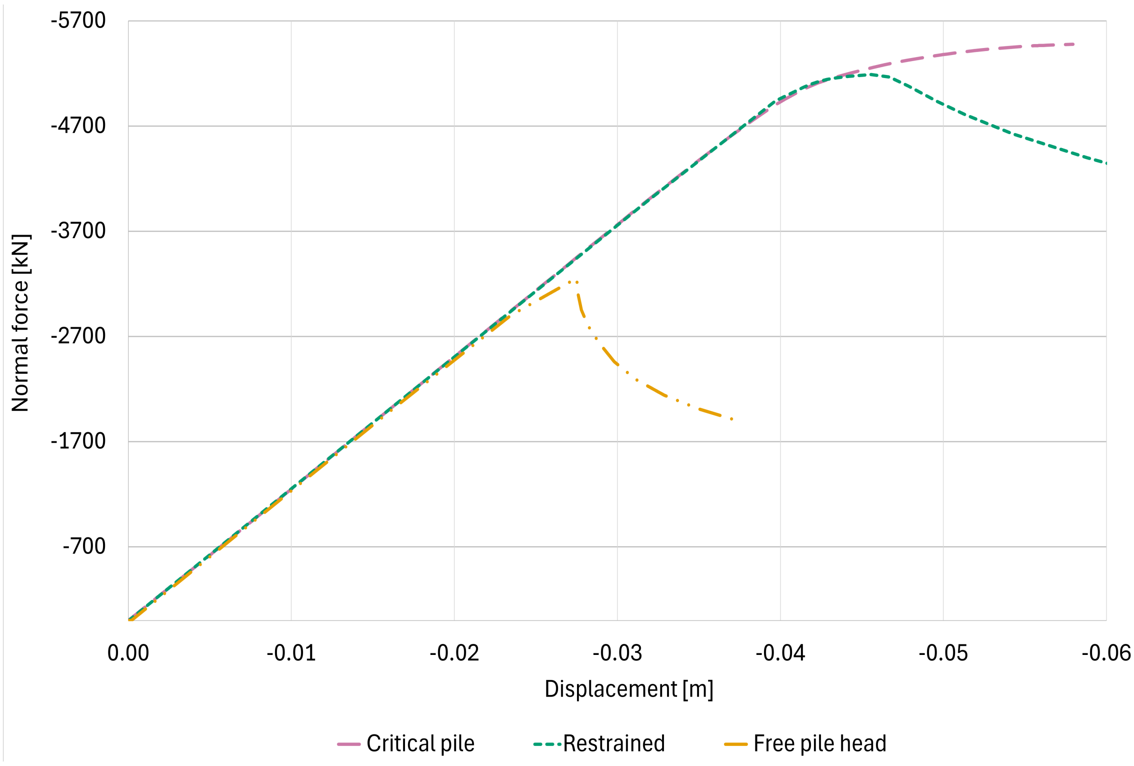

Figure 4.1: The correlation of normal force and deflection for piles surrounded by elastic-plastic sand.

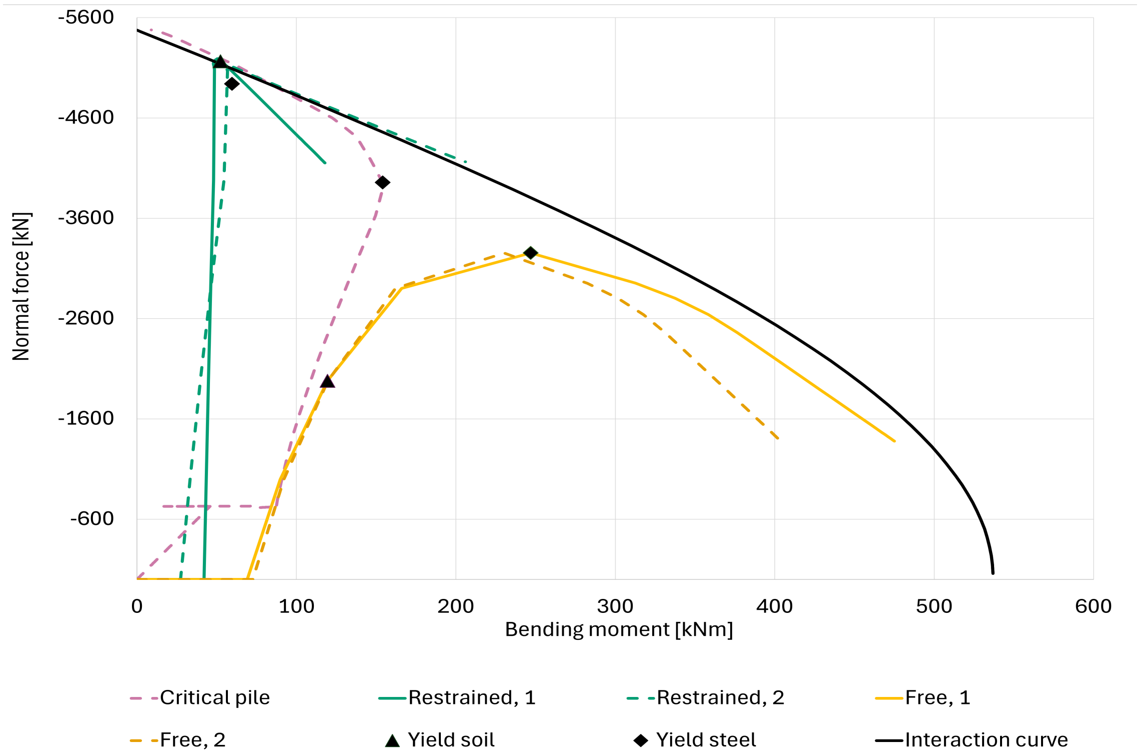

Figure 4.2: The correlation of normal force and bending moment for piles surrounded by elastic-plastic sand.

4.2.1 Redistribution mechanism of bending moment in stiff sand

The behaviour of the pile within the bridge system is governed by the stabilising effect of the surrounding stiff soil, which continues to provide lateral support even after the first plastic hinge forms. As the bending moment is redistributed along the pile, additional plastic hinges can develop sequentially. This redistribution mechanism increases the capacity of the pile before failure. Figure 4.3 illustrates the progression of moment migration as each hinge forms, showing how the structural system mobilises additional capacity through redistribution. Instability failure is not relevant for the stiff sand. In single pile cases, failure occurs shortly after steel hinge formation, whereas the bridge system enables redistribution of internal forces along the pile, delaying failure.

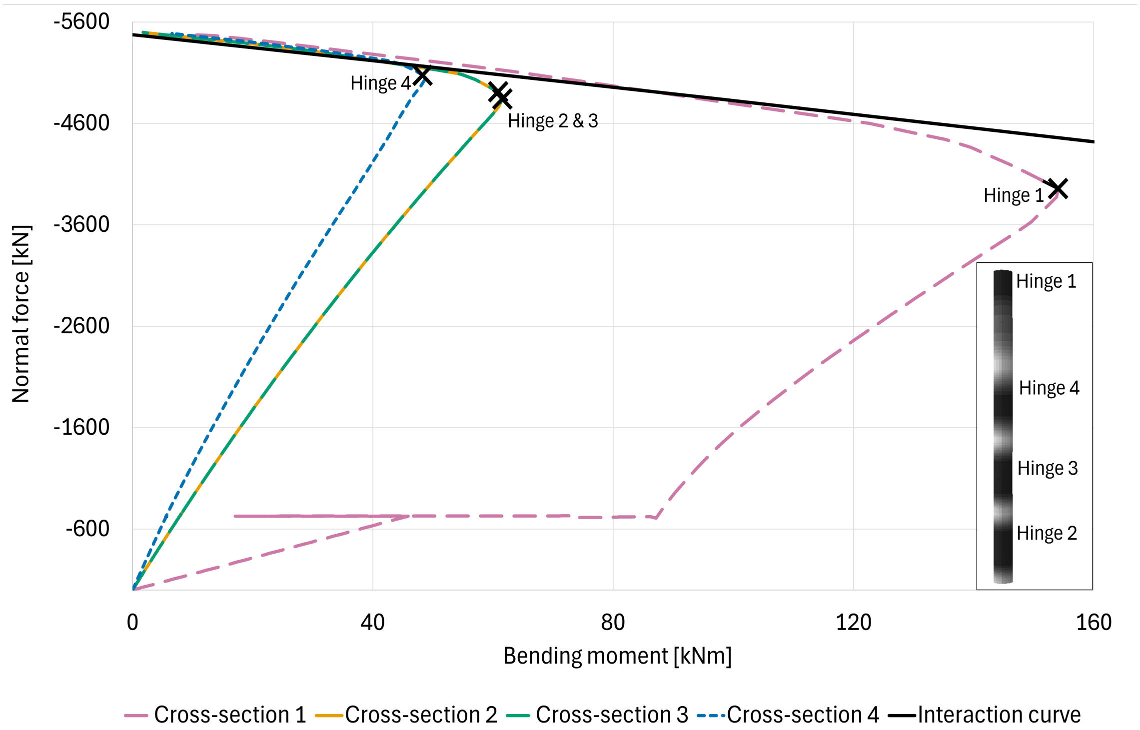

Figure 4.3: The correlation of normal force and bending moment in four cross-sections where hinges forms, showing progression of moment migration.

4.3 Evaluation of pile behaviour in fine-grained soil

Figures 4.4 and 4.5 present the response of single piles and the bridge system pile in fine-grained soil. Figure 4.4 illustrates the behaviour under loading in fine-grained soil, which can be compared to the behaviour observed in frictional soil in Figure 4.1. The normal force capacity for all piles in fine-grained soil is noted to be lower than in sand, and this trend is consistent in all comparative results for the two soils.

In Figure 4.5 it is observed that after the steel indicates yielding, the bridge pile and the restrained pile implies more capacity before failure. When the soil yields as well, the pile fails. For the pile with free pile head, the soil yields first and steel yielding causes failure. As observed in sand, Figure 4.2, the hinged pile head exhibits the maximum bending moment in the pile head due to the applied moment, and shifts location as the vertical force increases. However, this change is not identified in the pile within the bridge system or in the single pile with free pile head.

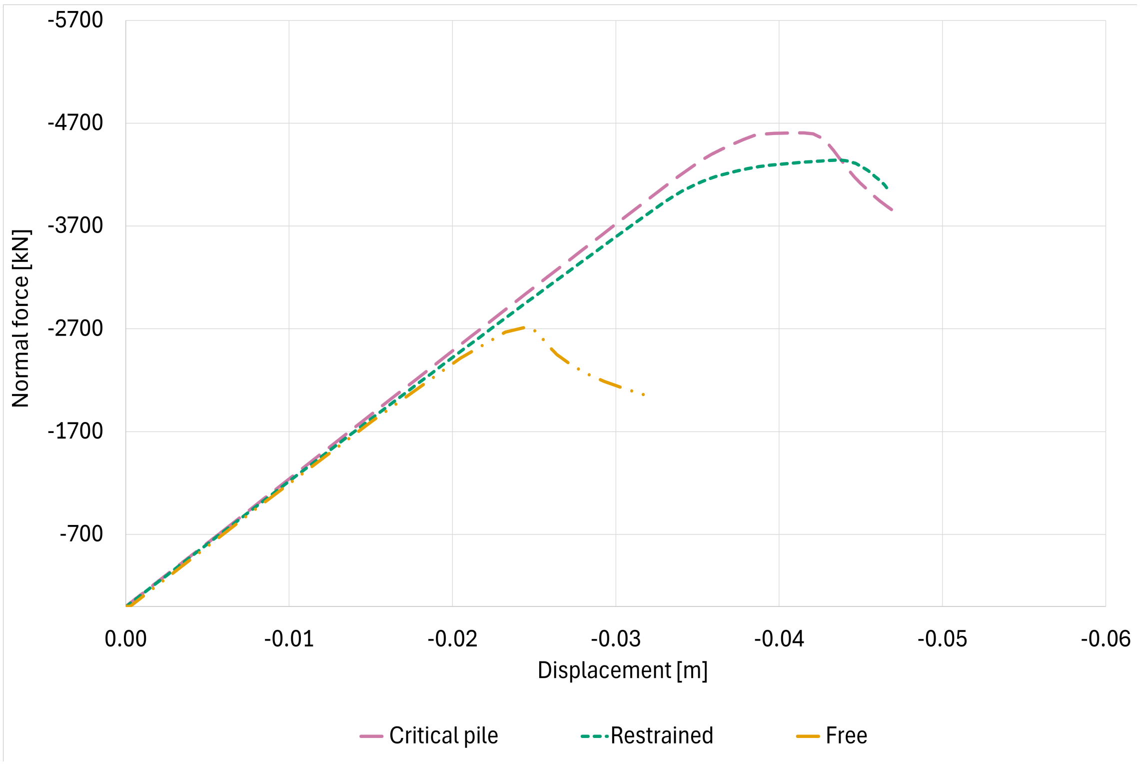

Figure 4.4: The correlation of normal force and deflection for piles surrounded by elastic-plastic fine-grained soil.

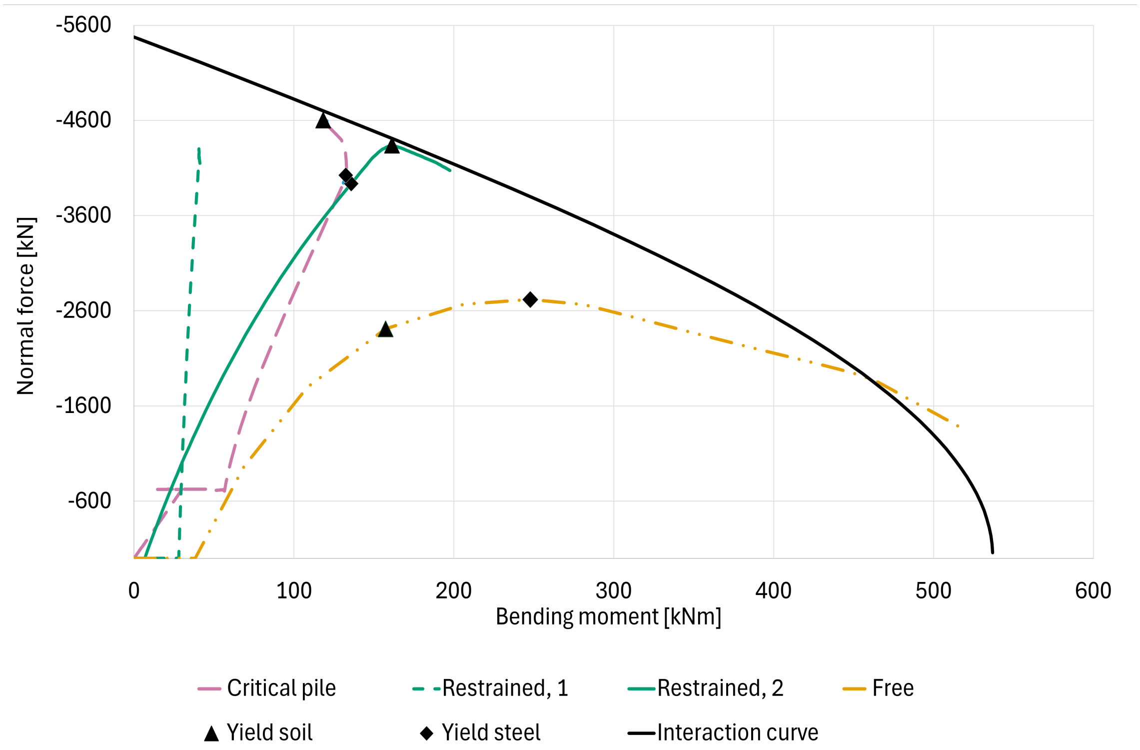

Figure 4.5: The correlation of normal force and bending moment for piles surrounded by elastic-plastic fine-grained soil.

4.3.1 Redistribution mechanism of bending moment in fine-grained soil

The critical pile in the bridge system embedded in fine-grained soil shows a redistribution mechanism similar to that observed in the stiff sand, although the extent of stabilisation differs. As plastic hinges begin to form, fine-grained soil provides limited but meaningful lateral support, allowing internal forces to be redistributed along the pile rather than causing failure.

Figure 4.6 illustrates the migration of moment moment as successive plastic hinges develop in the fine-grained soil profile. Despite the lower stiffness of the fine-grained soil, the structural system enables the pile to mobilise additional capacity beyond the initial hinge formation. Compared to the sand case, the response in fine-grained soil exhibits a more diffuse failure mechanism, where the redistribution of forces and the development of plastic hinges occur more gradually throughout the system. This suggests that even in a deformable soil environment, the bridge system facilitates a sequential yielding process, increasing the axial load capacity compared to isolated piles.

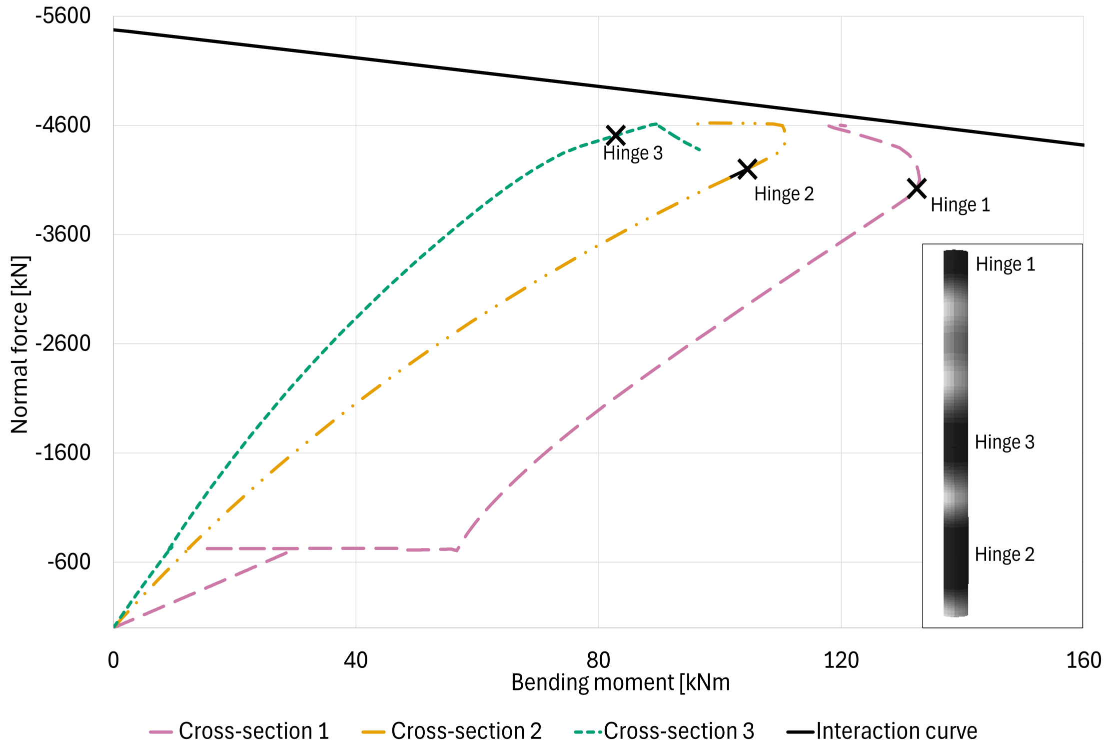

Figure 4.6: The correlation of normal force and bending moment in three cross-sections where hinges forms, showing progression of moment migration.

4.4 Discussion

The comparison between the free pile head and the hinged pile head highlights the importance of structural restraint. The free pile head consistently resulted in the lowest capacity due to larger lateral deformations and increased second-order effects. In contrast, the hinged pile head reduced the lateral displacements and delayed instability failure. The bridge system provided the greatest stabilising effect, as the connection between the piles and the bridge deck allowed several structural components to interact and redistribute forces after yielding in the steel pile had initiated.

Several simplifications were introduced in the numerical model. The soil was assumed to be homogeneous with constant material parameters, and the soil-structure interaction was represented using distributed springs based on p-y-curves and a Winkler foundation model. These assumptions simplify the complex behaviour of real soil conditions, where stiffness and strength vary with depth and load history.

In addition, the composite action between the steel tube and the concrete infill was neglected. This assumption reduces the bending stiffness of the piles and increases the predicted lateral deformations, leading to conservative estimates of second-order effects and buckling resistance. The results indicate that instability failure was not governing for the studied bridge system, particularly in the sand case where the relatively large pile diameter of 320 mm provided substantial lateral and bending stiffness. However, for longer and more slender piles founded in fine-grained soil, where the surrounding soil provides limited lateral support, buckling behaviour may become more critical.

Despite these simplifications, the sensitivity analyses and verification procedures indicate that the numerical model captures the overall structural behaviour realistically. The agreement between the FE model and the hand calculations, together with the expected deformation patterns and redistribution mechanisms, increases the reliability of the results obtained.

5

Conclusions

The results demonstrate that both soil stiffness and boundary conditions have a significant influence on the pile behaviour and load-carrying capacity. For all analysed cases, the critical pile within the integral bridge system exhibits a higher axial load carrying-capacity compared to the isolated single pile models. This indicates that the surrounding bridge structure contributes to improved system stability and increased axial stiffness, and enables redistribution of internal forces throughout the system.

The surrounding soil strongly influence the axial load capacity of the piles. In stiff coarse grained soils, the piles reach a higher capacity and a more concentrated redistribution of bending moments. Higher soil stiffness provide greater lateral support, reducing the probability of failure from instability and allowing the piles to reach the interaction curve, indicating failure in the pile material. In soft clay, the lower soil stiffness results in larger deformations and reduced capacity. However, the bridge system still allows redistribution of internal forces and sequential formation of plastic hinges, which increases the capacity compared to isolated pile cases. In single pile analyses, failure occurs shortly after the first plastic hinge formed. In the bridge system, the surrounding structure and the soil interaction allow additional plastic hinges to develop gradually along the pile. This redistribution mechanism delays failure and enables the mobilisation of additional capacity. The behaviour is especially noticeable in the friction soil case, where the soil continues to provide stabilising support after the local yielding in the steel starts.

The study demonstrates that modelling assumptions regarding soil stiffness and pile restraint significantly influence the predicted pile capacity in integral abutment bridges. Simplified single pile models may therefore underestimate the actual structural capacity of piles interacting with the bridge system. The results suggest that system interaction and redistribution effects should be considered in non-linear analyses of integral abutment bridges, especially when evaluating ultimate limit states and buckling behaviour. Therefore, future design practice should consider modelling piles with integrated boundary conditions and include soil-structure interaction in standardised calculation methods.

References

Ahn, J.-H., Yoon, J.-H., Kim, J.-H., & Kim, S.-H. (2011). Evaluation on the behavior of abutment–pile connection in integral abutment bridge. *Journal of Constructional Steel Research*, *67*(7), 1134–1148. https://doi.org/https://doi.org/10.1016/j.jcsr.2011.02.007

Eurocode – basis of structural design. (2002). *SIS*.

Eurokod 1: Laster på bärverk – del 1-5: Temperaturpåverkan. (2003). *SIS*.

Eurokod 1: Laster på bärverk – del 2: Trafiklaster på broar. (2003). *SIS*.

Fennema, J., Laman, J., & Linzell, D. (2005). Predicted and measured response of an integral abutment bridge. *Journal of Bridge Engineering*, *10*. https://doi.org/10.1061/(ASCE)1084-0702(2005)10:6(666)

Khodair, Y. A., & Hassiotis, S. (2005). Analysis of soil–pile interaction in integral abutment. *Computers and Geotechnics*, *32*(3), 201–209. https://doi.org/https://doi.org/10.1016/j.compgeo.2005.01.005

Liu, H., Han, J., & Parsons, R. L. (2022). Integral bridge abutments in response to seasonal temperature changes: State of knowledge and recent advances. *Frontiers in Built Environment*, *Volume 8 - 2022*. https://doi.org/10.3389/fbuil.2022.916782

Pålkommissionen. (2000). *Dimensioneringsprinciper för pålar* (Rapport 96:1). Pålkommissionen. https://www.palkommissionen.org/uploads/3200/96%20-1%20Dim.principer%20f%C3%B6r%20p%C3%A5lar.pdf

Pålkommissionen. (2006). *Transversalbelastade pålar – statiskt verkningssätt och dimensioneringsanvisningar* (Rapport 101). Pålkommissionen. https://www.palkommissionen.org/uploads/3407/101%20-Transversalbelastade%20p%C3%A5lar.pdf

Pålkommissionen. (2018). *Samverkanspålar av stål och betong* (Rapport 108). Pålkommissionen. https://www.palkommissionen.org/uploads/3182/108%20-%20Samverkansp%C3%A5lar%20av%20st%C3%A5l%20och%20betong.pdf

Trafikverket. (2011). *Trvr bro 11: Trafikverkets tekniska råd för brokonstruktion* (tech. rep. No. Publikation 2011:086). Trafikverket. Borlänge, Sweden.

A

Appendix A

Earth Pressure

Assumptions:

- Constant friction angle and unit weight of the soil
- Sand
- Groundwater table starts at 0 m
- Design Approach 3 (design values)
- Medium-dense relative density of the soil
- Elasto-plastic behavior in both the soil and the pile

Geometry

$D := 320\ \mathrm{mm}$ — Outer diameter pile

$t := 12.5\ \mathrm{mm}$ — Thickness piile

$L := 20\ \mathrm{m}$ — Length pile

$h_{äs} := 2.5\ \mathrm{m}$ — Height end screen

$b_{äs} := 5\ \mathrm{m}$ — Width end screen

$h_{vm1} := 1.1\ \mathrm{m}$ — Height 1 wind screen

$h_{vm2} := 2.5\ \mathrm{m}$ — Height 2 wind screen

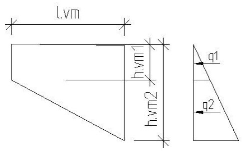

Material properties

$E_s := 210\ \mathrm{GPa}$ — E modulus steel

$f_{yk} := 460\ \mathrm{MPa}$ — Characterisc yield strength

$\gamma_{M0} := 1$ — Partial coefficient steel

$\mu_s := 1$ — Reduction factor

$f_{yd} := \dfrac{f_{yk}}{\gamma_{M0}} = 460\ \mathrm{MPa}$ — Dimensioning yield strength

Cross Section Characteristics

$D_i := D - 2 \cdot t = 295\ \mathrm{mm}$ — Inner diameter

$A := \pi \cdot \dfrac{D^2 - {D_i}^2}{4} = 12075.497\ \mathrm{mm}^2$ — Effective area

$I := \pi \cdot \dfrac{D^4 - {D_i}^4}{64} = 14296.256\ \mathrm{cm}^4$ — Moment of inertia

$W_{pl} := \dfrac{D^3 - {D_i}^3}{6} = 1182604.167\ \mathrm{mm}^3$ — Section modulus, plastic

$W_{el} := 2 \cdot \dfrac{I}{D} = 893516.006\ \mathrm{mm}^3$ — Section modulus, elastic

Soil properties

Pile

$\phi' := 34\ \mathrm{deg}$ — Friction angle (friction soil)

$\gamma_m := 1.3$ — Coefficient

End screen and wind screen

$\gamma_{flm} := 22\ \frac{kN}{m^3}$ Density backfill. TRVINFRA-00230 Table A1-1

$\gamma_{M.flm} := 1.3$ Partial safety factor drained analysis. TRVINFRA-00230, 6.2.7.1

$\phi_k := 45\ deg$ Characteristic friction angel. TRVINFRA-00230, Table A1-4

Earth pressure, friction soil

Pile

$z_\gamma := \begin{bmatrix} -20 \\ -16 \\ -12 \\ -8 \\ -4 \\ -2 \\ 0 \end{bmatrix} m$ z-levels of the pile

$\gamma' := \begin{bmatrix} 18 \\ 18 \\ 18 \\ 18 \\ 18 \\ 18 \\ 18 \end{bmatrix} \frac{kN}{m^3}$ Density of the soil

$z_c := -0\ m, -0.01\ m .. -20\ m$

$$\gamma(z) := \left\| \begin{array}{l} \text{if } z \le 0\ m \\ \quad \left\| \text{linterp}(z_\gamma, \gamma', z) \right. \\ \text{else} \\ \quad \left\| 0\ \frac{kN}{m^3} \right. \end{array} \right.$$

$\phi'_d := \text{atan}\left(\frac{\tan(\phi')}{\gamma_m}\right) = 27.423\ deg$ Design approch 3

$n_h := 4.5\ \frac{MN}{m^3}$ Medium-high relative density below the groundwater table TRVINFRA-00227, Appendix 3, Table 3-1

$n_{hd} := \frac{n_h}{\gamma_m} = 3.462\ \frac{MN}{m^3}$

$kd_{max} := \frac{12\ \frac{MN}{m^2} \cdot 0.6}{\gamma_m} = 5538.462\ \frac{\frac{kN}{m}}{m}$ Maximuml subgrade modulus for pile [spring/m]. TRVINFRA-00227, Appendix 3, Table 3-2. Sand

$\xi(z) := -z + 0\ m$ Conversion function between elevation (z-level) and soil depth

$kd(z) := min(n_{hd} \cdot \xi(z), kd_{max})$ Subgrade modulus for pile [spring /m]

$\sigma'_v(z) := -\int_{0\ m}^{z} \gamma'(z)\ dz$ Vertical stress as function of z-level

$K_{pd} := \tan\left(45\ deg + \frac{\phi'_d}{2}\right)^2 = 2.707$ Passive earth pressure, DA3

III

$q_d(z) := 3 \cdot K_{pd} \cdot \sigma'_v(z)$ Limit pressure [Pa]. Ekv 2.6 in PKR 101.

$Q_d(z) := q_d(z) \cdot D$ Limit pressure [kN/m]

$$y_d(z) := \begin{cases} \dfrac{Q_d(z)}{kd(z)} & \text{if } z < 0\ \mathrm{m} \\ 0\ \mathrm{m} & \text{else} \end{cases}$$

Displacement when limit pressure appears. Ekv 3.3.1a in PKR 96

Deflection vs depth

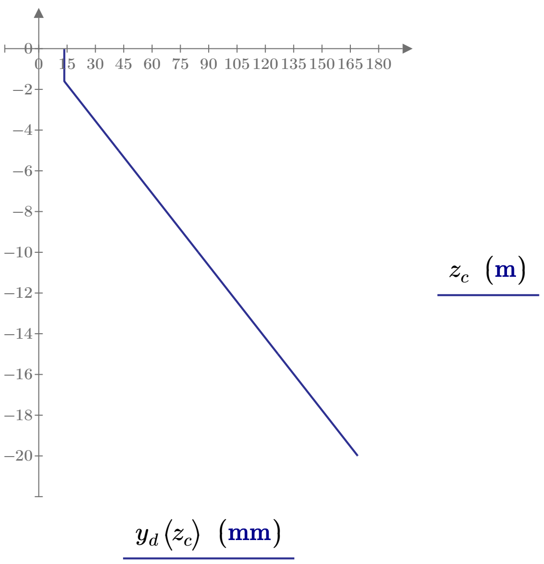

Limit pressure vs depth

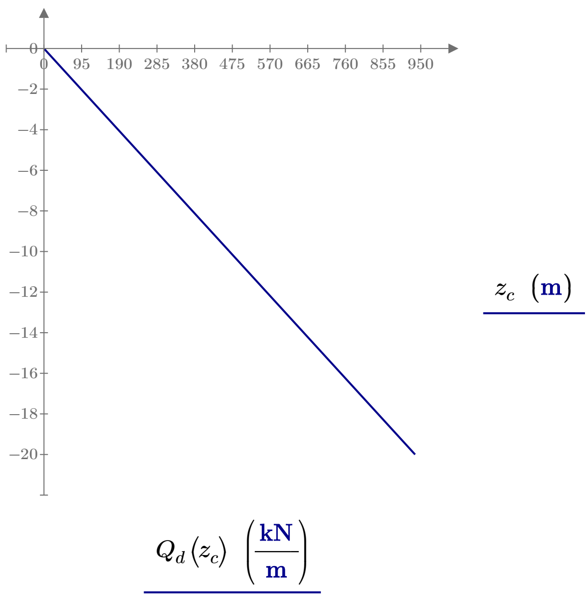

Sugrade reaction vs depth

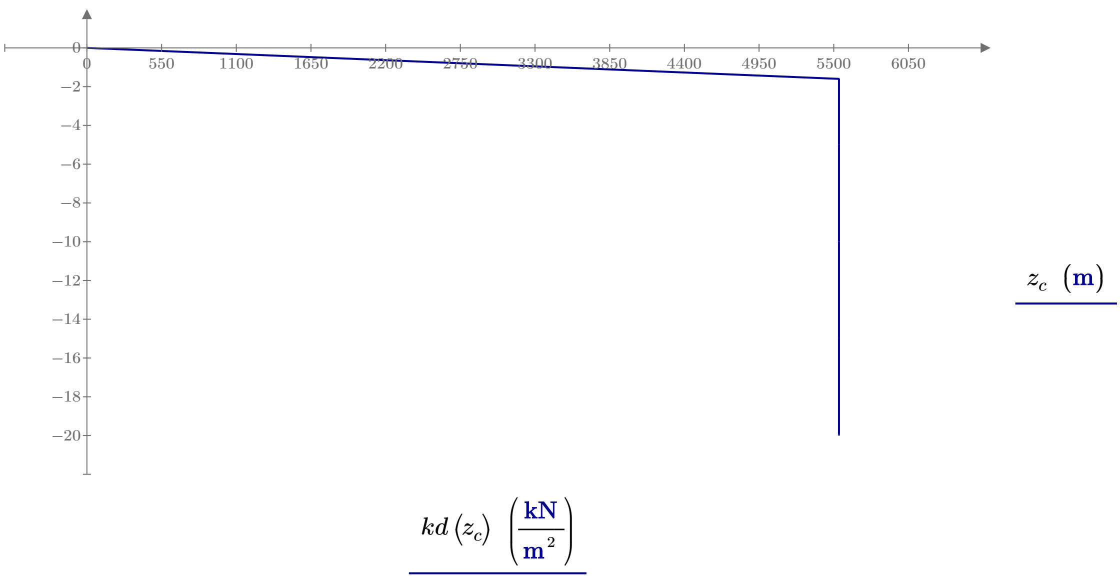

IV

Input data to Bridge Brigade.

$z_{brigade} := -0.5775\ \mathbf{m}, -2.7995\ \mathbf{m} .. -20.5775\ \mathbf{m}$

$$z_{brigade} = \begin{bmatrix} -0.578 \\ -2.8 \\ -5.022 \\ -7.244 \\ -9.466 \\ -11.688 \\ -13.91 \\ -16.132 \\ -18.354 \\ -20.576 \end{bmatrix} \mathbf{m} \qquad z_{mean} := \begin{bmatrix} -2.8+1.111 \\ -5.022+1.111 \\ -7.244+1.111 \\ -9.466+1.111 \\ -11.688+1.111 \\ -13.91+1.111 \\ -16.132+1.111 \\ -18.354+1.111 \\ -20.576+1.111 \end{bmatrix} \mathbf{m} = \begin{bmatrix} -1.689 \\ -3.911 \\ -6.133 \\ -8.355 \\ -10.577 \\ -12.799 \\ -15.021 \\ -17.243 \\ -19.465 \end{bmatrix} \mathbf{m}$$

$$\overrightarrow{Q_d(z_{mean})} = \begin{bmatrix} 79020 \\ 182978 \\ 286935 \\ 390892 \\ 494849 \\ 598806 \\ 702763 \\ 806720 \\ 910677 \end{bmatrix} \frac{\mathbf{N}}{\mathbf{m}} \qquad \overrightarrow{y_d(z_{mean})} = \begin{bmatrix} 0.014 \\ 0.033 \\ 0.052 \\ 0.071 \\ 0.089 \\ 0.108 \\ 0.127 \\ 0.146 \\ 0.164 \end{bmatrix} \mathbf{m}$$

End screen

Assumptions:

- Constant friction angle and unit weight of the soil
- Groundwater table starts at 0 m
- Design Approach 3
- Passive earth pressure is assumed to be fully mobilized when the total horizontal displacement toward the soil corresponds to 1/200 of the retaining wall height.

$\phi_d := \operatorname{atan}\left(\frac{\tan(\phi_k)}{\gamma_{M.flm}}\right) = 37.569\ \mathbf{deg}$ Dimensionerande friktionsvinkel i ULS

$K_{0.DA3} := 1 - \sin(\phi_d) = 0.39$ Coefficient at-rest earth pressure, DA3

$q_{äs.jord} := \gamma_{flm} \cdot K_{0.DA3} \cdot h_{äs} = 21465.908\ \mathbf{Pa}$ At-rest earth pressure

$K_{P.DA3} := \tan\left(45\ \mathbf{deg} + \frac{\phi_d}{2}\right)^2 = 4.124$ Passive earth pressure, DA3

$k_{äs} := \gamma_{flm} \cdot \frac{200}{h_{äs}} \cdot (K_{P.DA3} - K_{0.DA3}) \cdot \frac{h_{äs}}{2} = 8215.054\ \frac{\mathbf{kN}}{\mathbf{m}^3}$

$y_{äs} := \frac{h_{äs}}{200} = 0.013\ \mathbf{m}$ Maximum displacement

$q_{äs} := \frac{h_{äs}}{200} \cdot k_{äs} = 102688.174\ \mathbf{Pa}$ Limit pressure

Wing wall

$n_{h.v} := 18 \; \frac{\mathrm{MN}}{\mathrm{m}^3}$

Very high relative density below the groundwater table. TRVINFRA-00227, Appendix 3, Tabel 3-1

$h_{mean} := \frac{h_{vm1} + h_{vm2}}{2} = 1.8 \; \mathrm{m}$

$k_{vm} := \gamma_{flm} \cdot \frac{200}{h_{mean}} \cdot \left(K_{P.DA3} - K_{0.DA3}\right) \cdot \frac{h_{mean}}{2} = \left(8.215 \cdot 10^3\right) \; \frac{\mathrm{kN}}{\mathrm{m}^3}$

$y_{vm} := \frac{h_{mean}}{200} = 0.009 \; \mathrm{m}$

Maximum displacement

$q_{vm} := \frac{h_{mean}}{200} \cdot k_{vm} = 73935.486 \; \mathrm{Pa}$

Limit pressure

Subgrade modulus, soil

$\alpha_{lt} := 50\%$

50% permanent load

$c_{ud} := 20 \; \mathrm{kPa}$

$kd_{soil} := 50 \cdot c_{ud} = 1000 \; \mathrm{kPa}$

Subgrade modulus for pile

$q_{d.soil} := \left(9 - 3 \cdot \alpha_{lt}\right) \cdot c_{ud} = 150 \; \mathrm{kPa}$

Limit pressure [Pa]

$Q_{d.soil} := q_{d.soil} \cdot D = 48000 \; \frac{\mathrm{N}}{\mathrm{m}}$

Limit pressure [kN/m]

$y_d := \frac{Q_{d.soil}}{kd_{soil}} = 0.048 \; \mathrm{m}$

Displacement [mm]

Initial imperfection, soil

$l_k := \pi \cdot \sqrt[4]{E_s \cdot \frac{I}{kd_{soil}}} = 7.354 \; \mathrm{m}$

Critical buckling length. PKR 96 supplement 2 page 8

$\delta_k := \frac{l_k}{600} = 12.256 \; \mathrm{mm}$

Characteristic imperfection

$\gamma_d := 2.0$ *No control of straightness*

Partial coefficient. PKR 96 supplement 2 page 8

$\delta_d := \delta_k \cdot \gamma_d = 24.513 \; \mathrm{mm}$

Dimensioning imperfection

$\delta_{fb} := 0.0013 \cdot l_k = 9.56 \; \mathrm{mm}$

Residual stresses, group b

$\delta_0 := \delta_{fb} + \delta_d = 0.03407 \; \mathrm{m}$

Total dimensioning imperfection

B

Appendix B

Loads

Deadweight

Coating

$\gamma_{coat} := 23 \frac{\mathrm{kN}}{\mathrm{m}^3}$ TRVINFRA-00227, 7.1.6.1.1

$t_{coat} := 110\ \mathrm{mm}$ Thickness coating

$q_{coat} := \gamma_{coat} \cdot t_{coat} = 2.53\ \mathrm{kPa}$

Shrinkage

SS-EN 1992-1-1 Chapter 3.1.4

$\alpha_{ds1} := 4$ $\alpha_{ds2} := 0.12$ Cement class N

$f_{ck} := 35\ \mathrm{MPa}$

$f_{cm} := f_{ck} + 8\ \mathrm{MPa} = 43\ \mathrm{MPa}$

$f_{cm0} := 10\ \mathrm{MPa}$

$RH := 80$

$RH_0 := 100$

$$\beta_{RH} := 1.55 \cdot \left(1 - \left(\frac{RH}{RH_0}\right)^3\right) = 0.756$$

$$\varepsilon_{cd.0} := 0.85 \cdot \left(\left(220 + 110 \cdot \alpha_{ds1}\right) \cdot \exp\left(-\alpha_{ds2} \cdot \frac{f_{cm}}{f_{cm0}}\right)\right) \cdot 10^{-6} \cdot \beta_{RH} = 0$$

$A_c := 5.7\ \mathrm{m}^2$

$u := 6.76\ \mathrm{m}$

$$h_0 := \frac{2\ A_c}{u} = 1.686\ \mathrm{m}$$

$k_h := 0.7$

$\varepsilon_{cd} := k_h \cdot \varepsilon_{cd.0} = 0$

$$\varepsilon_{ca} := 2.5 \cdot \left(\frac{f_{ck}}{\mathrm{MPa}} - 10\right) \cdot 10^{-6} = 0$$

$\varepsilon_{cs} := \varepsilon_{cd} + \varepsilon_{ca} = 0$

$$\alpha_T := 10^{-5} \frac{1}{\mathrm{K}}$$

VIII

$T_{cs} := \frac{\varepsilon_{cs}}{\alpha_T} = 23.98\ \mathrm{K}$

Temperature

SS-EN 1991-1-5, Chapter 6

$T_{max} := 36\ \mathrm{°C}$ $\quad T_{min} := -38\ \mathrm{°C}$ TSFS 2018:57 Skara

$T_0 := 10\ \mathrm{°C}$ Casting temperature

Corrected values, SS-EN 1991-1-5, 6.1.3.1. Figure 6.1

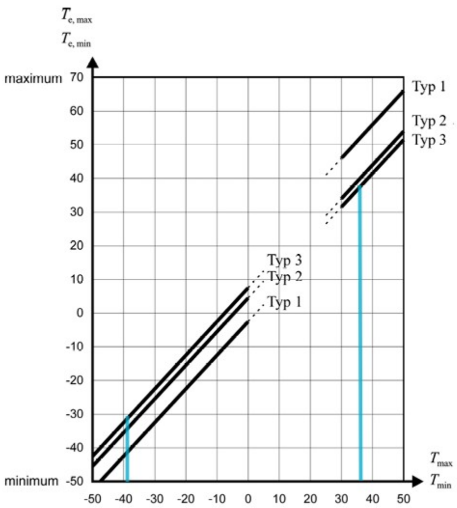

$T_{e.max} := 38\ \mathrm{°C}$

$T_{e.min} := -30\ \mathrm{°C}$

$\Delta T_{N.cool} := T_{e.min} - T_0 = -40\ \mathrm{K}$ Temperature difference for contraction

$\Delta T_{N.heat} := T_{e.max} - T_0 = 28\ \mathrm{K}$ Temperature difference for expansion

$\Delta T_N := T_{e.max} - T_{e.min} = 68\ \mathrm{K}$ Total temperature difference

Temperature difference

$\Delta T_{M.heat} := 15\ \mathrm{K}$ Upper side warmer then lower side

$\Delta T_{M.cool} := 8\ \mathrm{K}$ Lower side warmer then upper side

$k_{sur.heat} := 0.5 + 0.2 \cdot \frac{(150\ \mathrm{mm} - t_{coat})}{150\ \mathrm{mm} - 100\ \mathrm{mm}} = 0.66$ Coefficient to account for the coat layer, SS-EN 1991-1-5, tabel 6.2

$k_{sur.cool} := 1$

$\boxed{\Delta T_{M.heat}} := \Delta T_{M.heat} \cdot k_{sur.heat} = 9.9\ \mathrm{K}$ Upper side warmer than lower side

$\boxed{\Delta T_{M.cool}} := \Delta T_{M.cool} \cdot k_{sur.cool} = 8\ \mathrm{K}$ Lower side warmer than upper side

Load combination

$\omega_M := 0.75$ $\omega_N := 0.35$

Case 1:	$\Delta T_{N.cool} = -40\ \mathrm{K}$	$\Delta T_{M.cool} \cdot \omega_M = 6\ \mathrm{K}$
Case 2:	$\Delta T_{N.cool} = -40\ \mathrm{K}$	$\Delta T_{M.heat} \cdot \omega_M = 7.425\ \mathrm{K}$
Case 3:	$\Delta T_{N.heat} = 28\ \mathrm{K}$	$\Delta T_{M.cool} \cdot \omega_M = 6\ \mathrm{K}$
Case 4:	$\Delta T_{N.heat} = 28\ \mathrm{K}$	$\Delta T_{M.heat} \cdot \omega_M = 7.425\ \mathrm{K}$
Case 5:	$\Delta T_{N.cool} \cdot \omega_M = -30\ \mathrm{K}$	$\Delta T_{M.cool} = 8\ \mathrm{K}$
Case 6:	$\Delta T_{N.cool} \cdot \omega_M = -30\ \mathrm{K}$	$\Delta T_{M.heat} = 9.9\ \mathrm{K}$
Case 7:	$\Delta T_{N.heat} \cdot \omega_M = 21\ \mathrm{K}$	$\Delta T_{M.cool} = 8\ \mathrm{K}$
Case 8:	$\Delta T_{N.heat} \cdot \omega_M = 21\ \mathrm{K}$	$\Delta T_{M.heat} = 9.9\ \mathrm{K}$

Wind

SS-EN 1991-1-4:2005

$h_{bridge.edge} := 600\ \mathrm{mm}$ Height bridge edge

$\rho_a := 1.25\ \dfrac{\mathrm{kg}}{\mathrm{m}^3}$ Density air

$v_b := 24\ \dfrac{\mathrm{m}}{\mathrm{s}}$ Reference wind velocity. TSFS, 2018_57, Figure 7.1, Skara

$q_p := 0.73\ \mathrm{kPa}$ TSFS, 2018_57, Table 7.1 for terrain type II and =8m

$q_b := \dfrac{1}{2} \cdot \rho_a \cdot {v_b}^2 = 0.36\ \mathrm{kPa}$ Reference velocity pressure. SS -EN 1991-1-4, chapter 4.5

$c_c := \dfrac{q_p}{q_b} = 2.028$ SS -EN 1991-1-4, chapter 4.5

$d_{öb} := 1.33\ \mathrm{m}$ Mean height affected by wind

$d_{traffic} := 2\ \mathrm{m}$ Height traffic

$d_{tot} := d_{öb} + d_{traffic} = 3.33\ \mathrm{m}$ Total height from lower edge bridge to upper edge traffic

$b_{bro} := 5.8\ \mathrm{m}$ Width superstructure

$\dfrac{b_{bro}}{d_{tot}} = 1.742$

X

$$c_{fx.0} := min\left(\begin{array}{l}\text{if } \dfrac{b_{bro}}{d_{tot}} > 5 \\ \quad \| 1 \\ \text{else if } \dfrac{b_{bro}}{d_{tot}} < 5 \\ \quad \left\| \left(1 + 0.3 \cdot \left(5 - \dfrac{b_{bro}}{d_{tot}}\right)\right) \right. \\ \text{else} \\ \quad \| 2.4 \end{array}\right) = 1.977$$

SS -EN 1991-1-4. Figure 8.3

$c_{fx} := c_{fx.0} = 1.977$

$C := c_c \cdot c_{fx} = 4.01$

Form factor

$q_w := q_b \cdot C = 1.444\ \mathbf{kPa}$

Wind load on bridge and traffic. SS -EN 1991-1-4. Eq 8.2

$q_{w.bridge.edge} := q_w \cdot d_{tot} = 4.807\ \dfrac{\mathbf{kN}}{\mathbf{m}}$

Traffic load

SS-EN 1991-2:2003

Load model 1 is used for this case.

Load model 1 (LM1)

SS-EN 1991-2, 4.3.2, figure 4.2a.

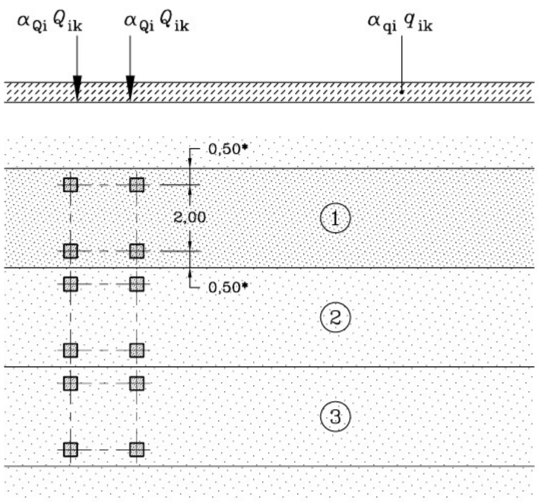

Only load area 1, since road is less than 5.4m

$\alpha_{Q1} := 0.9$ $\alpha_{Q2} := 0.9$ $\alpha_{Q3} := 0$

Adjustment factors. TSFS 2018:57. Table 11.1

$\alpha_{q1} := 0.8$ $\alpha_{qi} := 1$ $\alpha_{qr} := 1$

$Q_{1k} := 300\ \mathrm{kN} \cdot \alpha_{Q1} = 270\ \mathrm{kN}$ Axial load, load area 1

$Q_{k.övrigt} := 0\ \mathrm{kN}$ Other load areas

$Q_{k.återstående} := 0\ \mathrm{kN}$ Other area

$q_{1k} := 9\ \dfrac{\mathrm{kN}}{\mathrm{m}^2} \cdot \alpha_{q1} = 7.2\ \mathrm{kPa}$ Distributed load, load area 1

$q_{k.övrigt} := 2.5\ \dfrac{\mathrm{kN}}{\mathrm{m}^2} \cdot \alpha_{qr} = 2.5\ \mathrm{kPa}$ Other load areas

$q_{k.återstående} := 2.5\ \dfrac{\mathrm{kN}}{\mathrm{m}^2} \cdot \alpha_{qr} = 2.5\ \mathrm{kPa}$ Other area

Braking / accelearation

Load model 1

SS-EN 1991-2, 4.4.1

$Q_{1k} := 300\ \mathrm{kN}$

$q_{1k} := 9\ \dfrac{\mathrm{kN}}{\mathrm{m}^2}$

$\alpha_{Q1} = 0.9$

$\alpha_{q1} = 0.8$

$w_1 := 3\ \mathrm{m}$ Width load field

$L_{bridge} := 1.5\ \mathrm{m} + 17\ \mathrm{m} + 1.5\ \mathrm{m} = 20\ \mathrm{m}$ Distance from end screen to end screen (back edge)

$Q_{bk} := 0.6 \cdot \alpha_{Q1} \cdot (2 \cdot Q_{1k}) + 0.1 \cdot \alpha_{q1} \cdot q_{1k} \cdot w_1 \cdot L_{bridge} = 367.2\ \mathrm{kN}$

Standard vehicle

2018:57, 11 kap, 2§

$Q_{v.typfordon} := (0.44 + 1.32 + 0.44 + 1.32) \cdot 300\ \mathrm{kN} = 1056\ \mathrm{kN}$

$Q_{b.typfordon} := min\,(0.35 \cdot Q_{v.typfordon}, 500\ \mathrm{kN}) = 369.6\ \mathrm{kN}$

$Q_{bk} := \max\,(Q_{b.typfordon}, Q_{bk}) = 369.6\ \mathrm{kN}$ Critical braking force

$\dfrac{Q_{bk}}{2} = 184.8\ \mathrm{kN}$ Load in brigade, two point loads

$q_{bk} := \dfrac{Q_{bk}}{L_{bridge}} = 18.48\ \dfrac{\mathrm{kN}}{\mathrm{m}}$

Lateral load

$Q_{trk} := Q_{bk} \cdot 0.25 = 92.4\ \mathrm{kN}$

Surcharge load

$q_{eq.öv} := 10\ \frac{kN}{m^2}$ $\qquad$ $q_{eq.6m} := 20\ \frac{kN}{m^2}$

$K_{0.DA3} := 0.39$ — Coefficient at-rest earth pressure, DA3. (From Chapter Earth Pressure)

$q_{öl.öv.DA3} := q_{eq.öv} \cdot K_{0.DA3} = 3.9\ kPa$

$q_{öl.6m.DA3} := q_{eq.6m} \cdot K_{0.DA3} = 7.8\ kPa$

$q_{basic} := q_{öl.öv.DA3} = 3.9\ kPa$ — "Basic pressure" in Brigade

$L_{LW} := 6\ m$ — "Load width" in Brigade

$q_{LVI} := (q_{eq.6m} - q_{eq.öv}) \cdot L_{LW} = 60\ \frac{kN}{m}$ — "Vertical load intensity" in Brigade

$L_S := 0$ — "Load spread" in Brigade, no load distribution in depth

$b_{äs} := 5\ m$ — Width end screen

$h_{äs} := 2.5\ m$ — Height end screem

$q_{öl} := q_{öl.6m.DA3} = 7.8\ kPa$ — End screen width less than 6 meter

$\Delta P_{öl} := q_{öl} \cdot h_{äs} \cdot b_{äs} = 97.5\ kN$

$\Delta q_{öl} := \Delta P_{öl} \cdot \frac{2}{h_{äs} \cdot b_{äs}} = 15.6\ kPa$

$k_{äs} := (8.215 \cdot 10^3)\ \frac{kN}{m^3}$ — (Chapter Earth Pressure)

$\delta_{öl} := \frac{\Delta q_{öl}}{k_{äs}} = 1.899\ mm$

C

Appendix C

Normal and Moment Capacity for Laterally Restrained Pile

Loaded with normal force

Input data

$E_s := 210\ \mathrm{GPa}$ — E modulus steel. (Appendix Earth Pressure)

$I := 14296.3\ \mathrm{cm}^4$ — Moment of inertia. (Appendix Earth Pressure)

$A := 12075\ \mathrm{mm}^2$ — Effective area. (Appendix Earth Pressure)

$W_{pl} := 1182604.167\ \mathrm{mm}^3$ — Section modulus, plastic. (Appendix Earth Pressure)

$\mu_s := 1$ — Reduction factor. (Appendix Earth Pressure)

$f_{yd} := 460\ \mathrm{MPa}$ — Dimensioning yield strength. (Appendix Earth Pressure)

$Q_d := 75\ \dfrac{\mathrm{kN}}{\mathrm{m}}$ — Limit pressure at 1.6m when kdd constant. (Appendix Earth Pressure)

$k_d d := 5500\ \mathrm{kPa}$ — Modulus of subgraded reaction, kN/m/m. (Appendix Earth Pressure)

Capacity of normal force and moment in steel pile

PKR 96. Supplement 2

$N_{Rd} := \mu_s \cdot A \cdot f_{yd} = \left(5.555 \cdot 10^3\right)\ \mathrm{kN}$

$\alpha_m := 1$

$M_{Rd} := \alpha_m \cdot W_{pl} \cdot f_{yd} = 543.998\ \mathrm{kN \cdot m}$

Critical buckling load

$P_k := 2 \cdot \sqrt{k_d d \cdot E_s \cdot I} = 25699.982\ \mathrm{kN}$ — PKR 96

Initial imperfection

$l_k := \pi \cdot \sqrt[4]{E_s \cdot \dfrac{I}{k_d d}} = 4.802\ \mathrm{m}$ — Critical buckling length. PKR 96 supplement 2 page 8

$\delta_k := \dfrac{l_k}{600} = 8.003\ \mathrm{mm}$ — Characteristic imperfection

$\gamma_d := 2.0$ *No control of straightness* — Partial coefficient. PKR 96 supplement 2 page 8

$\delta_d := \delta_k \cdot \gamma_d = 16.007\ \mathrm{mm}$ — Dimensioning imperfection

$\delta_{fb} := 0.0013 \cdot l_k = 6.243\ \mathrm{mm}$ — Residual stresses, group b

$\delta_0 := \delta_{fb} + \delta_d = 0.02225\ \mathrm{m}$ — Total dimensioning imperfection

Load effect in pile with subgraded modulus. Elastic response in soil

PKR 84a eq. 42

$P_k := 2 \cdot \sqrt{k_d d \cdot E_s \cdot I} = 25699.982\ \mathrm{kN}$ — Maximum allowable axial force as a function of additional deflection

$y := 2\ \mathrm{mm}$ — Starting test value

$$P(y) := \frac{y \cdot P_k}{\delta_0 + y}$$

Load at which the limit value of soil resistance is reached. PKR 84a eq. 41.

$$M_{Ed}(y) := \frac{0.5 \cdot P(y) \cdot \delta_0}{1 - \frac{P(y)}{P_k}}$$

PKR 84a, eq. 39. Dimensioning moment

$$y_0 := \text{root}\left(\left(\frac{P(y)}{N_{Rd}} + \frac{M_{Ed}(y)}{M_{Rd}}\right) - 1, y\right) = 5.204\ \text{mm}$$

Finding maximum deflection

$$\frac{P(y_0)}{N_{Rd}} + \frac{M_{Ed}(y_0)}{M_{Rd}} = 100\%$$

$$M_{Ed}(y_0) = 66.872\ \text{kN} \cdot \text{m}$$

Total moment capacity

$$P(y_0) = 4871.703\ \text{kN}$$

Total normal capacity

Load effect in pile with subgraded modulus.
Plastic response in soil, elastic in pile

$$y := 0.00001\ \text{mm}, 1\ \text{mm} .. 100\ \text{mm}$$

$$\alpha(y) := \text{asin}\left(\frac{y_b}{y}\right)$$

PKR 84a Eq. 49

$$\Phi(y) := \text{if}\left(y < y_b, 1, \frac{2}{\pi} \cdot \left(\alpha(y) + 1.5 \cdot \sin(2 \cdot \alpha(y)) - (\pi - 2 \cdot \alpha(y)) \cdot \sin(\alpha(y))^2\right)\right)$$

PKR 84a, ekv 47

$$P_{k1}(y) := P_k \cdot \Phi(y)$$

$$P(y) := \frac{y \cdot P_{k1}(y)}{\delta_0 + y}$$

PKR 84a Eq. 41

$$M(y) := \frac{0.5 \cdot P(y) \cdot \delta_0}{1 - \frac{P(y)}{P_{k1}(y)}}$$

PKR 84a Eq. 39

$$y_b := \frac{Q_d}{k_d d} = 13.64\ \text{mm}$$

Deflection at limit pressure

$$P(y_b) = 9765.898\ \text{kN}$$

Normal force at limit pressure

$$M(y_b) = 175.227\ \text{kN} \cdot \text{m}$$

Moment at limit pressure

Elastic capacity of pile

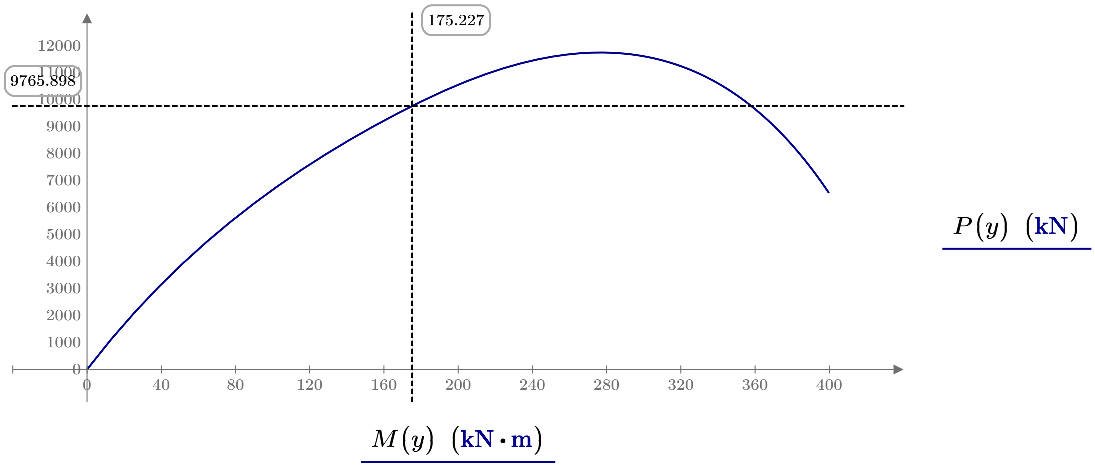

Deflection vs normal force in pile

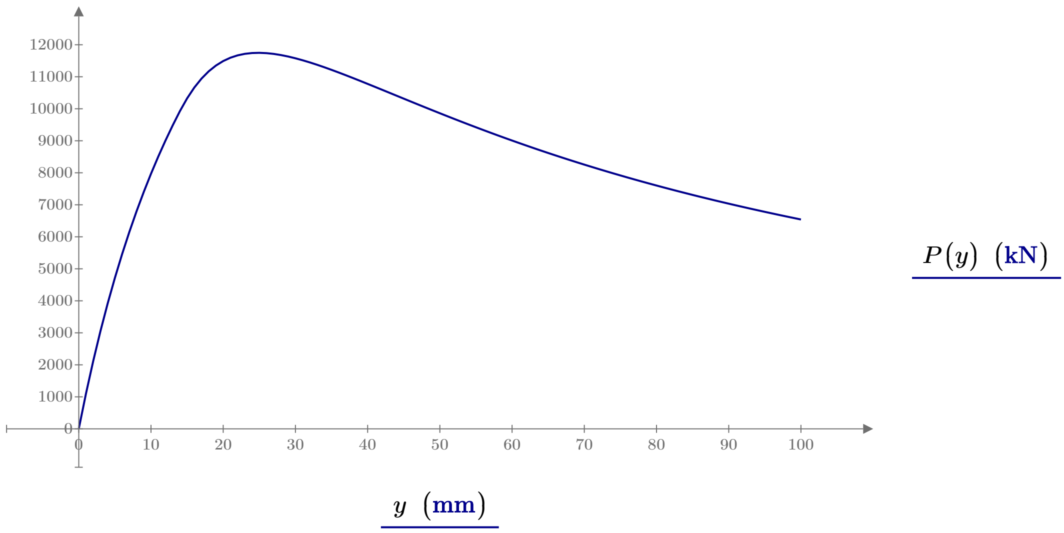

D

Appendix D

Normal and Moment capacity for Pile with Free Pile Head

Loaded with horizontal and normal force

Input data

$E_s := 210\ \mathrm{GPa}$	E modulus steel. (Appendix Earth Pressure)
$D := 320\ \mathrm{mm}$	Diameter pile
$L := 20\ \mathrm{m}$	Length pile
$I := 14296.3\ \mathrm{cm}^4$	Moment of inertia. (Appendix Earth Pressure)
$A := 12075\ \mathrm{mm}^2$	Effective area. (Appendix Earth Pressure)
$W_{pl} := 1182604.167\ \mathrm{mm}^3$	Section modulus, plastic (Appendix Earth Pressure)
$\mu_s := 1$	Reduction factor. (Appendix Earth Pressure)
$f_{yd} := 460\ \mathrm{MPa}$	Dimensioning yield strength. (Appendix Earth Pressure)
$Q_d := 75\ \dfrac{\mathrm{kN}}{\mathrm{m}}$	Limit pressure at 1.6m when subgrade reaction is constant.
$k_d d := 5500\ \mathrm{kPa}$	Modulus of subgraded reaction, kN/m/m. (Appendix Earth Pressure)

Critical normal force and moment for steel pile

PKR 96. Supplement 2

$$N_{Rd} := \mu_s \cdot A \cdot f_{yd} = \left(5.555 \cdot 10^3\right)\ \mathrm{kN}$$

$$\alpha_m := 1$$

$$M_{Rd} := \alpha_m \cdot W_{pl} \cdot f_{yd} = 543.998\ \mathrm{kN \cdot m}$$

Critical buckling load

$$P_k := \sqrt{k_d d \cdot E_s \cdot I} = 12849.991\ \mathrm{kN}$$

Theoretical normal force. PKR 101, figure 3.6

Effects of horizontal load

$$V_{max} := 43\ \mathrm{kN}$$

Test value, horizontal force

$$L_{cr} := \sqrt[4]{\frac{4 \cdot E_s \cdot I}{k_d d}} = 2.16\ \mathrm{m}$$

Critical buckling length

$$z := 0\ \mathrm{m}, 10\ \mathrm{mm} .. 2 \cdot \pi \cdot L_{cr}$$

$$\delta(z) := e^{\frac{-z}{L_{cr}}} \cdot \cos\left(\frac{z}{L_{cr}}\right)$$

Shape function for beam deformation on an elastic foundation

$$y_h(z) := \frac{2 \cdot V_{max}}{k_d d \cdot L_{cr}} \cdot \delta(z)$$

Deflection on level z

$$z_{y\_0mm} := \frac{L_{cr} \cdot \pi}{2} = 3.396\ \mathrm{m}$$

Depth when y=0mm

$$y_h\left(z_{y\_0mm}\right) = 0\ \mathrm{mm}$$

$$y_{h.lin}(z) := -y_h(0\ \mathrm{m}) \cdot \frac{(z - z_{y\_0mm})}{z_{y\_0mm}}$$

Straight line function

$$y_{h\_max} := 25.979\ \mathrm{mm}$$

Deflection due to horizontal load

Deflection of pile vs depth

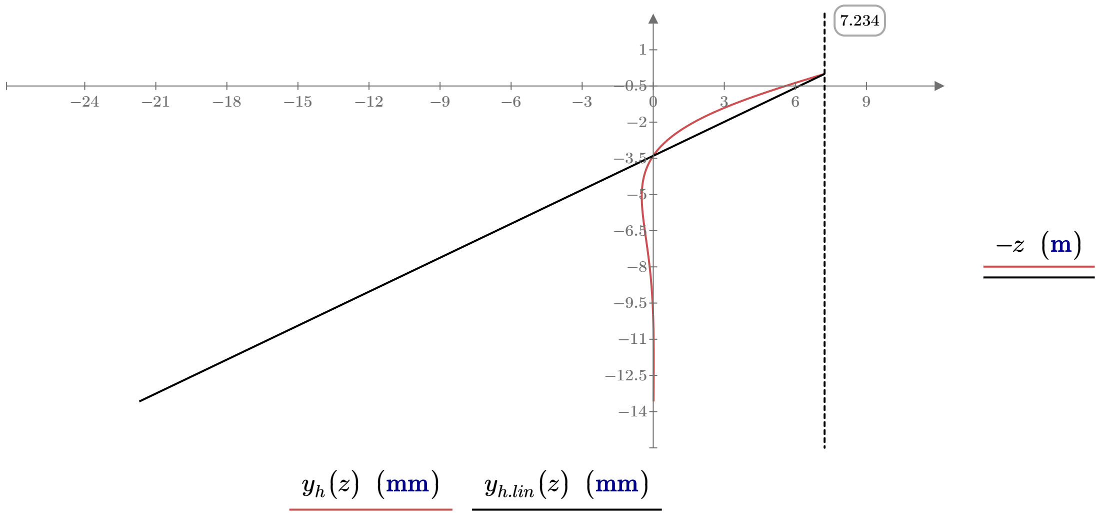

$$\delta_h(z) := y_{h.lin}(z) - y_h(z)$$

Fictitious initial imperfection caused by additional deflection due to lateral loading

$$z_{max\_\delta h} := \frac{L_{cr} \cdot \pi}{4} = 1.7\ \mathrm{m}$$

Depth at maximum difference of δ_h

$$\delta_h := \delta_h(z_{max\_\delta h}) = 1.3\ \mathrm{mm}$$

Addition to initial imperfection

$$\beta(z) := e^{\frac{-z}{L_{cr}}} \cdot \sin\left(\frac{z}{L_{cr}}\right)$$

Variation of bending moment with depth (elastic foundation). PKR 96, s52

$$M(z) := V_{max} \cdot L_{cr} \cdot \beta(z)$$

Function of moment with depth. PKR 96, s52

$$z_{M.max} := \frac{L_{cr} \cdot \pi}{4} = 1.70\ \mathrm{m}$$

Depth at maximum moment

$$\Delta M := M(z_{M.max}) = 30.0\ \mathrm{kN \cdot m}$$

Additional moment due to horizontal load

Moment in pile based on depth

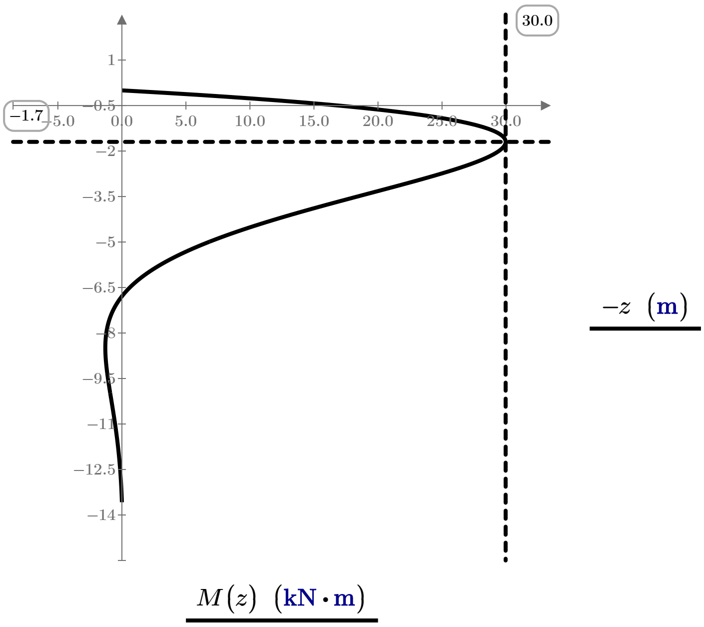

Initial imperfection

$l_k := \pi \cdot \sqrt[4]{E_s \cdot \frac{I}{k_d d}} = 4.802 \text{ m}$ — Critical buckling length. PKR 96 supplement s.8

$\delta_k := \frac{l_k}{600} = 8.003 \text{ mm}$ — Characteristic imperfection

$\gamma_d := 2.0$ *No control of straightness* — Partial coefficient. PKR 96 supplement s.8

$\delta_d := \delta_k \cdot \gamma_d = 16.007 \text{ mm}$ — Dimensioning imperfection

$\delta_{fb} := 0.0013 \cdot l_k = 6.243 \text{ mm}$ — Residual stresses, Grupp b

$\delta_0 := \delta_{fb} + \delta_d + \delta_h = 23.534 \text{ mm}$ — Total dimensioning imperfection, hand calculation

Load effect in pile with subgraded modulus

$y_b := \frac{Q_d}{k_d d} = 13.6364 \text{ mm}$ — Additional deflection when limit pressure

$y_{h\_max} = 25.979 \text{ mm}$ — Deflection due to horizontal load. Less than 75mm, elastic respons

$y := 25.979 \text{ mm}, 27 \text{ mm} .. 100 \text{ mm}$

$\alpha(y) := \operatorname{asin}\left(\frac{y_b}{y}\right)$ — PKR 84a ekv 49

$\Phi(y) := \text{if}\left(y < y_b, 1, \frac{2}{\pi} \cdot \left(\alpha(y) + 1.5 \cdot \sin(2 \cdot \alpha(y)) - (\pi - 2 \cdot \alpha(y)) \cdot \sin(\alpha(y))^2\right)\right)$ PKR 84a ekv 47

$P(y) := 2 \cdot \sqrt{k_d d \cdot E_s \cdot I \cdot \Phi(y)} \cdot \frac{y}{\delta_0 + y}$ PKR 108 Eq 3.21.

$M(y) := \frac{P(y) \cdot (\delta_0 + y)}{2}$ Moment due to normal force. PKR 108 Eq 3.20.

$P(y_b) = 9428.363\ \mathbf{kN}$ Maximum normal force before plastic respons from soil

$M(y_b) = 175.227\ \mathbf{kN \cdot m}$ Maximum moment before plastic respons from soil

Elastic capacity of pile

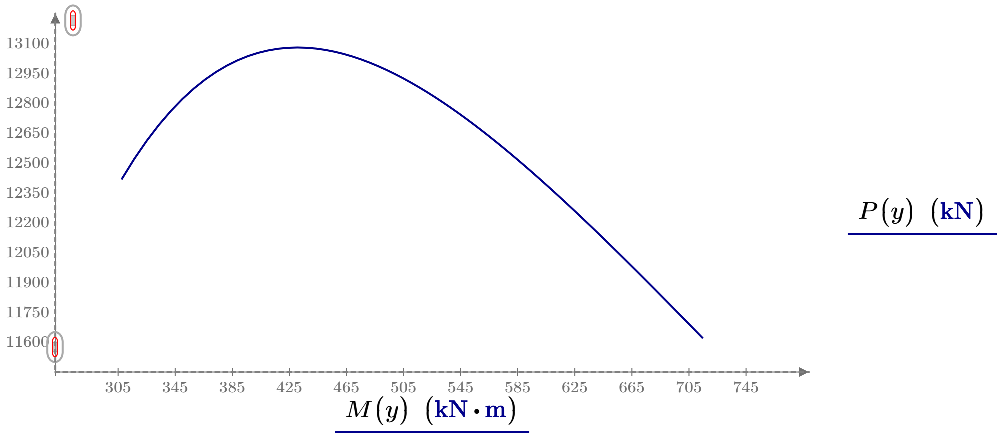

E

Appendix E

Verify behaviour of end screen and pile for horizontel force

Input data

$Q_{bk} := 369.6\ \mathrm{kN}$	(Appendix Loads)
$h_{äs} := 2.5\ \mathrm{m}$	Height end screen
$b_{äs} := 5\ \mathrm{m}$	Width end screen
$E_s := 210\ \mathrm{GPa}$	E modulus steel.
$I := 14296.3\ \mathrm{cm}^4$	Moment of inertia. (Appendix Earth Pressure)
$k_d d := 5500\ \mathrm{kPa}$	Modulus of subgraded reaction, kN/m/m. (Appendix Earth Pressure)
$k_{äs} := 8215.054\ \dfrac{\mathrm{kN}}{\mathrm{m}^3}$	(Appendix Earth Pressure)

Verfiying that the end screen and piles act as expected with regard to spring stiffness

$$Q_{bk.red} := Q_{bk} \cdot 0.63 = 232.848\ \mathrm{kN}$$

Deflection on end screen. No spring stiffness in piles. Load: Breaking force

$$\delta_{break} := \frac{Q_{bk.red}}{k_{äs} \cdot h_{äs} \cdot b_{äs}} = 2.268\ \mathrm{mm}$$

$$y_{brigade.endscreen} := 2.67\ \mathrm{mm}$$

Applied force

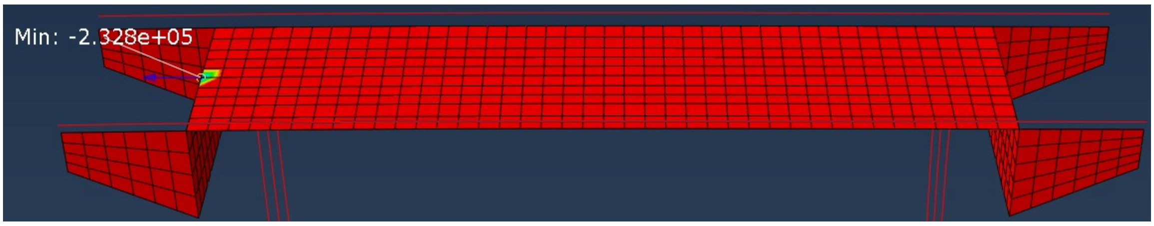

Deflection

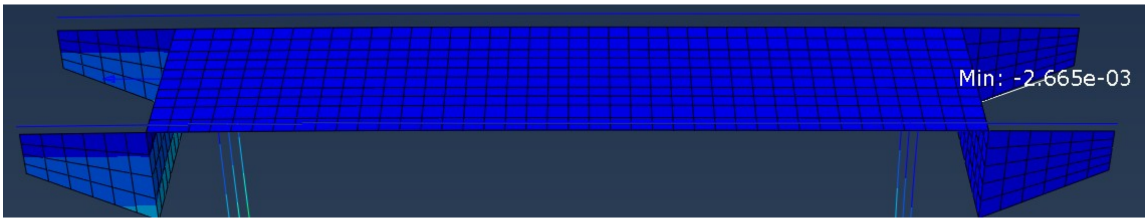

Deflection of one pile. No spring stiffness in end screens.
Free pile head. Load: 39kN

For piles subjected to combined axial and transverse loading, the interaction effects shall be considered. Two methods for this are presented in Pålkommissionens Rapport 96, Section 4.3. Method 2 is selected.

$$V := \frac{Q_{bk.red}}{6} = 38.808\ \mathbf{kN}$$

Maximum transverse load at pile head

$$L_{cr} := \sqrt[4]{\frac{4 \cdot E_s \cdot I \cdot 1}{k_d d}} = 2.16\ \mathbf{m}$$

Critical length. SS-EN 1994-2, 6.7.3.4 (2).

$$\delta(z) := e^{\frac{-z}{L_{cr}}} \cdot \cos\left(\frac{z}{L_{cr}}\right)$$

Shape function for beam deformation on an elastic foundation

$$y_h(z) := \frac{2 \cdot V}{k_d d \cdot L_{cr}} \cdot \delta(z)$$

$$y_h(0\ \mathbf{m}) = 6.528\ \mathbf{mm} \qquad y_{brigade.pile} := 6.6\ \mathbf{mm}$$

Applied force

Deflection

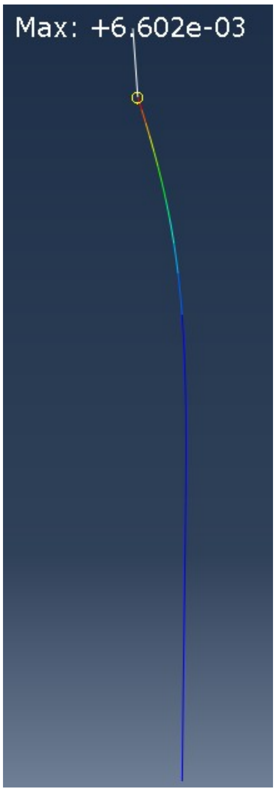

DEPARTMENT OF SOME SUBJECT OR TECHNOLOGY
CHALMERS UNIVERSITY OF TECHNOLOGY
Gothenburg, Sweden
www.chalmers.se

AVANCEZ
1829
CHALMERS
UNIVERSITY OF TECHNOLOGY